Max-Planck-Institut
für Meteorologie

REPORT No. 316

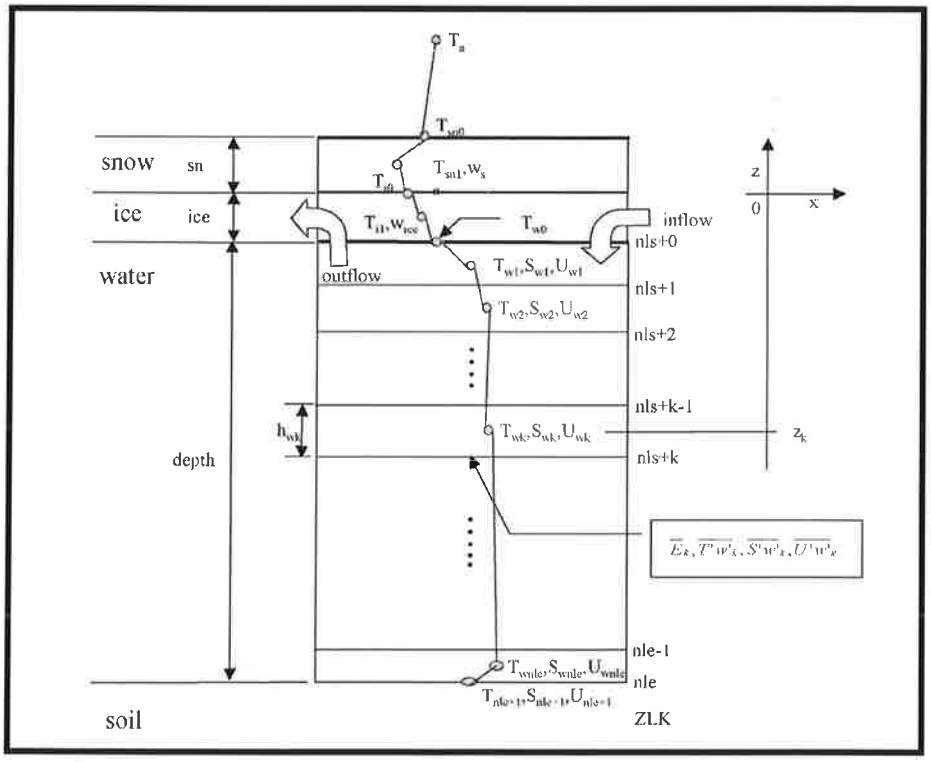

LAKE PARAMETERIZATION FOR CLIMATE MODELS

by

Ben-Jei Tsuang • Chia-Ying Tu • Klaus Arpe

HAMBURG, March 2001

AUTHORS:

Ben-Jei Tsuang — Dept. of Environmental Engineering, Nat'l Chung-Hsing University, Taichung, Taiwan

Chia-Ying Tu, Klaus Arpe — Max-Planck-Institut für Meteorologie, Hamburg, Germany

MAX-PLANCK-INSTITUT
FÜR METEOROLOGIE
BUNDESSTRASSE 55
D-20146 HAMBURG
F.R. GERMANY

Tel.: +49 - (0)40 - 411 73 - 0
Telefax: +49 - (0)40 - 411 73 - 298
E-Mail: <name>@dkrz.de

ISSN 0937 – 1060

Lake Parameterization for Climate Models

Ben-Jei Tsuang

Dept. of Environmental Engineering
Nat'l Chung-Hsing University
Taichung, Taiwan

Chia-Ying Tu, Klaus Arpe

Max-Planck-Institut für Meteorologie
Hamburg, Germany

ISSN 0937 – 1060

Contents

1. Introduction

A lake parameterization is developed for climatic models. The scheme is especially designed to simulate the skin temperature of a lake grid at various stages, such as the stages of an evolution of a thermocline, potential ice formation/destruction, and snowfall/snowmelt on the ice. It is basically an one column model with a good vertical resolution. It can deal with salt and fresh water. The only forcing on the lake model comes from the atmosphere model. For great lake, e.q. the Caspian Sea, also some horizontal exchange between neighboring grid point is in the model.

In order to develop a general lake model for a climatic model, we have to consider the characteristics of all the large lakes in the world. The most important lakes include the Caspian Sea and the Great Lakes. The Caspian Sea occupies six connected grids points in T42 resolution, and the Great Lakes two-separated grid points (DKRZ, 1994). The Caspian Sea is a terminal saline lake. It covers 393,000 km^2 with depths varying from few meters in the north and 1000 m in the south. The Volga River supplies the largest river discharge of 7260 m^3 s^{-1} to the lake (0.77 m yr^{-1} in increase of sea level of the Caspian Sea). The North Caspian freezes over every year and a greater part of it is covered with pack ice during the winter (Kosarev and Yablonskaya, 1994). Skin temperature is a key variable to couple with an atmospheric model. In order to simulate the skin temperature of a lake such as the Caspian Sea, temperature of water, ice and snow, salinity, current as well as turbulent kinetic energy are simulated in the model. The ice forms when the water skin temperature reaches the freezing point, and the time of ice melt and snowmelt occurs when their skin temperatures raise to the freezing point, respectively. A theory presented here is to simulate the skin temperature including periods of snow cover, ice cover and open water. Different to ocean models, the lake model is very sensitive to the water level. The model presented here pays special attention to water level calculation.

2. Theory

2.1. Coordinate System

The coordinate system of the lake routine is geo-potential $\tilde{z}$ -coordinate. $\tilde{z}$ is in geo-potential meter (gpm). $\Delta\tilde{z}$ (gpm) = $\rho \cdot \Delta z / \rho_0$ (kg m^{-3} m / kg m^{-3}) where ρ_0 = 1000 kg m^{-3}. Each lake grid in the same lake has the same reference $\tilde{z}$ -coordinate system ZLK(0) - ZLK(18) as shown in Figure 1. The water is divided into 18 layers. The boundaries of each layer are at depths of 0, 1, 2, 4, 8, 10, 12, 14, 16, 18, 20, 40, 60, 80, 100, (wlvlref-100)-(depth-100)/3, (wlvlref-100)-(depth-100)*2/3 and (wlvlref – depth) gpm, where "wlvlref" is a reference water level (-28 m for the Caspian Sea and 176 m for the Great Lakes); depth is the maximum depth of a lake (589 m for the Caspian Sea and 62 m for the Great Lakes inT42 resolution). Subroutine "lkcord" is used to maintain the reference coordinate.

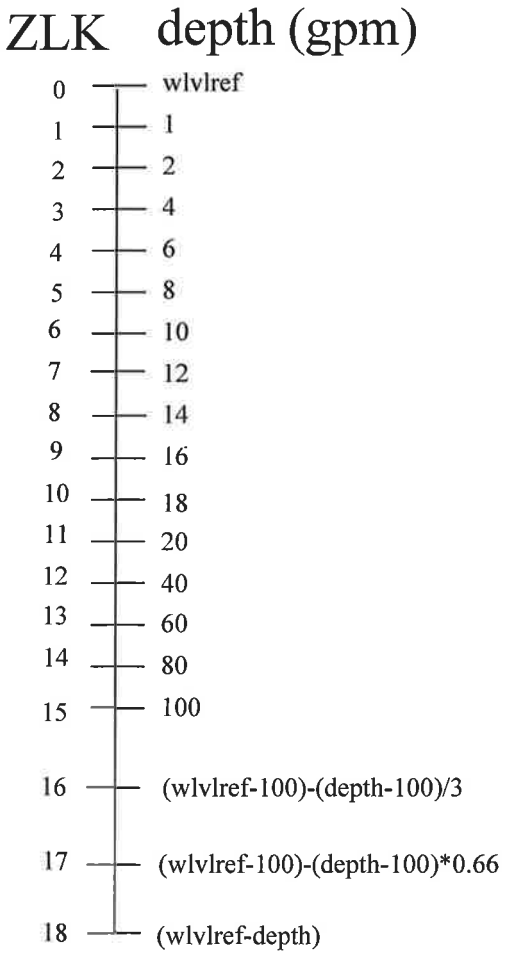

Figure 1 Schematic of a lake reference coordinate system.

In the vertical coordinate system of lake model, "nls" is the first water level and "nle" is the last water level of the lake grid. ZLK(0)-ZLK(nls) of each lake grid are further set to be the current water level (wlvl) of each grid if the original values of reference coordinates ZLK(0)-ZLK(nls) are higher than wlvl. In addition, if "wlvl" is higher than "wlvlref", ZLK(0) is set to be "wlvl". Note that "wlvlref" is a reference water level and "wlvl" is current water level. Futhermore, ZLK(nle)-ZLK(18) is set to be the lake bed of each grid if the original values of ZLK(nle)-ZLK(18) are lower than "topo" (bathymeter of a lake grid). Note that ZLK(nls) and ZLK(nle) of different lake grid of the same lake need not to be the same. Figure 2 shows a schematic of the algorithm. Subroutine "pzcord" is used to calculate the coordinate system of each lake grid.

Moreover, over a water grid there lies one ice layer and one snow layer. Figure 3 shows a schematic of vertical diffusion of temperature (T), salinity (S), current (U) and liquid water (W). T_{sn0} is skin temperature of snow, T_{i0} is skin temperature of ice, $T_{w,nls+0}$ is skin temperature of water, T_{nle+1} is skin temperature of soil ($=T_g$) underneath of a water column. T_{sn1} is mean temperature of snow, T_{i1} is mean temperature of ice and $T_{w,nls+k}$ is mean water temperature at layer k of a water column.

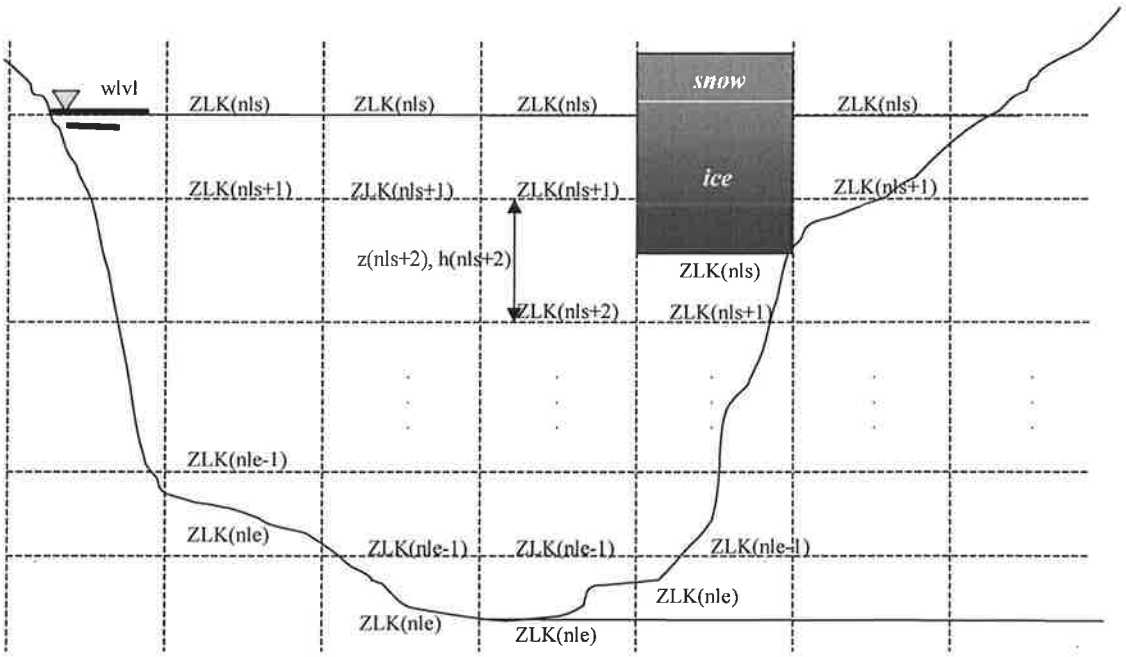

Figure 2 Schematic of a lake coordinate system.

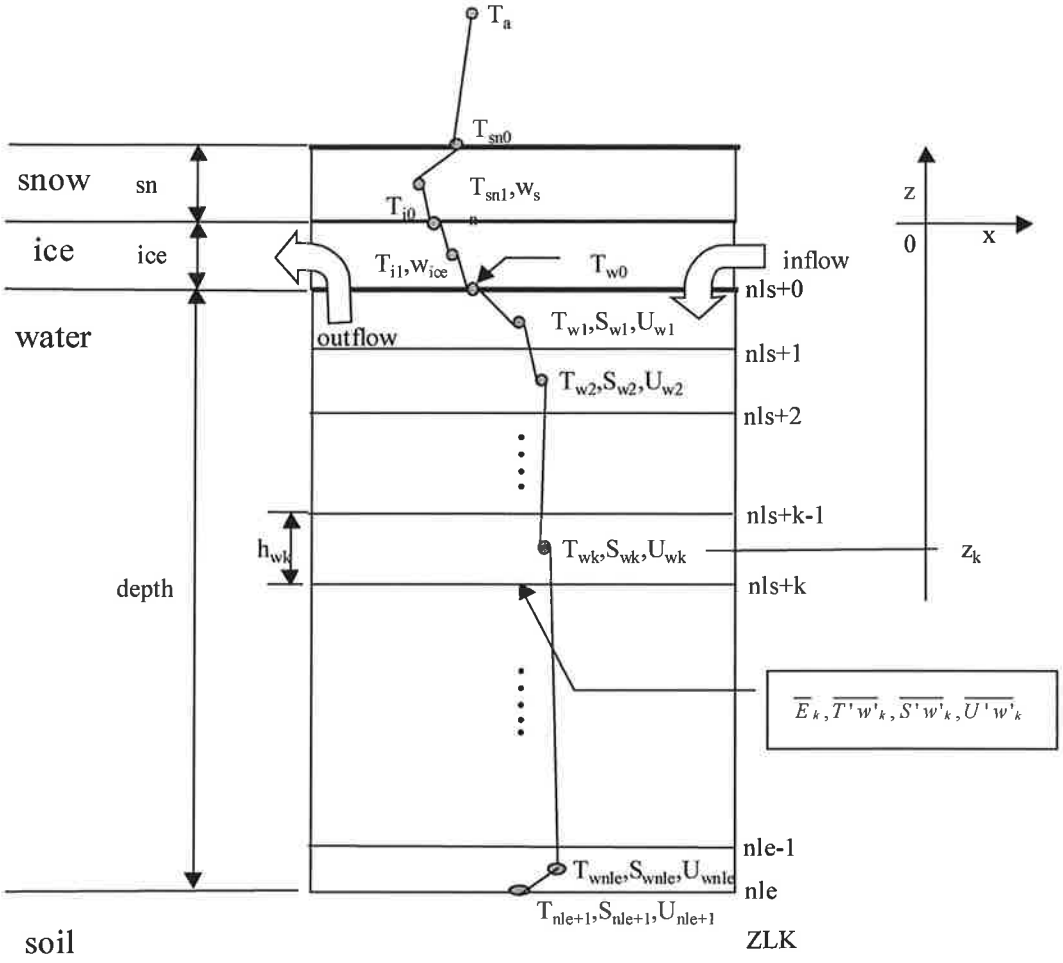

Figure 3 Vertical discretization of a lake grid.

2.2. Model Physics

2.2.1. Snow Period

While a lake is covered with snow, the energy budget of a snow pack is a balance among net solar radiation, non-solar energy flux at the snow surface, phase change energy due to snow melt and refreeze, and heat conduction to the underneath ice. The energy conservation equation is written as:

$$\rho_w c_{sn} sn \frac{\partial T_{sn1}}{\partial t} = R_{sn} - Q_{ns} - \left(sm - wfs \right) \rho_w \left[L_w + c_{sn} \left(T_{0°C} - T_{sn1} \right) \right] - \rho_{sn} c_{sn} k_{sn} \frac{T_{sn1} - T_{i0}}{h_{sn} / 2} \quad (1)$$

where sn is the snow depth of dry snow in water equivalent (m), $sn = h_{sn} \rho_{sn} / \rho_w$; R_{sn} is net solar radiation (w m^{-2}), Q_{ns} is non-solar energy flux (w m^{-2}), sm is the

melting rate of a snow pack (m s^{-1}), wfs is the freezing rate of liquid water inside a snow pack (m s^{-1}). Q_{ns} includes atmospheric longwave radiation, terrestrial longwave radiation, sensible heat, latent heat and advection energy due to snowfall and rain. It is:

$$Q_{ns} = -R_{ld} + \sigma T_s^4 + H + LE - rain\,\rho_w\left[c_w\left(T_{rain} - T_{0°C}\right)\right] - snowfl\,\rho_w\left[c_{sn}\left(T_{snowfl} - T_{sn}\right)\right] \quad (2)$$

where the temperature of liquid water in snow is fixed to $T_{0°C}$. The mass and energy of rain advect to liquid water in snowpack. The mass and energy of snowfall advect to snowpack.

The mass conservation equations for dry snow and liquid water in the snow pack are determined as:

$$\frac{\partial sn}{\partial t} = snowfl - sm + wfs - E \quad (3a)$$

$$\frac{\partial wsn}{\partial t} = rain + sm - wfs - u_{sw} \quad (3b)$$

where wsn is the liquid water content in the snow pack (m), E is sublimation rate (m s^{-1}) and u_{sw} is the rate of movement of liquid water in snow to the underneath ice. It is assumed sublimation taking from the dry snow portion. The rate of liquid water movement u_{sw} can be determined by Darcy's law as (Jordan, 1983a, 1983b; March and Woo, 1985):

$$u_{sw} = \alpha k_s S^{*3} \quad (4)$$

where α is a constant (= 5.47 E6 m^{-1} s^{-1} at 0℃), k_s is snow permeability (m^2) and S^* is effective water saturation (dimensionless). They are determined from Shimizu's (1970) equation (Colbeck and Anderson, 1982; Tsuang, 1990) as:

$$k_s = 0.077 g_s^{\,2} \exp\left(-7.8\rho_{sn}/\rho_w\right) \quad (5)$$

$$S^* = \frac{(\theta - \theta_i)}{(\phi - \theta_i)} \quad (6)$$

where g_s is grain size of snow (0.9 mm is used in this study) (Colbeck and Anderson, 1982). ϕ is porosity ($1 - \rho_{sn}/\rho_{ice}$). θ_i is irreducible water content (5% is used in this study). θ is liquid water content ($= \frac{wsn}{sn(\rho_w/\rho_{sn})}$).

2.2.2. Iced Period

Similarly, the energy conservation equations for snow-free ice is:

$$\rho_w c_{ice} ice \frac{\partial T_{ice}}{\partial t} = R_{sn} - Q_{ns} - \left(\dot{im} - \dot{wfi} - \dot{icf} \right) \rho_w \left[L_w + c_{ice} \left(T_{0°C} - T_{ice} \right) \right] - \rho_{ice} c_{ice} k_{ice} \frac{T_{ice} - T_{w0}}{h_{ice} / 2} \tag{7}$$

and

$$Q_{ns} = -R_{ld} + \sigma T_s^4 + H + LE - \dot{rain} \rho_w \left[c_w \left(T_{rain} - T_{0°C} \right) \right] \tag{8}$$

where ice is the dry ice depth in water equivalent (m), $sn = h_{sn} \rho_{sn} / \rho_w$; $\dot{im}$ is the melting rate of a ice pack, $\dot{wfi}$ is the freezing rate of liquid water within the ice pack and $\dot{icf}$ is the ice formation rate due to the frozen of the underneath water, respectively (m s^{-1}).

The mass conservation equation for ice pack is determined as:

$$\frac{\partial ice}{\partial t} = -\dot{im} + \dot{wfi} + \dot{icf} - E \tag{9a}$$

$$\frac{\partial wice}{\partial t} = \dot{rain} + u_{sw} + \dot{im} - \dot{wfi} - u_{iw} \tag{9b}$$

where $wice$ is the liquid water content within an ice pack (m), E is sublimation rate (m s^{-1}) and u_{iw} is rate of movement of liquid water within ice to the underneath water body. It is assumed sublimation taking from the dry ice portion. The rate of liquid water movement u_{iw} is parameterized as:

$$u_{iw} = \left(wice - wice_{mx} \right) / \Delta t \tag{10}$$

where $wice_{mx}$ is a maximum threshold of liquid water over ice (set to be 0.01 m in this study).

2.2.3. Open Water Period

Similarly, the energy conservation equations for open water can be written as:

$$\rho_w c_w h_{w1} \frac{\partial T_{w1}}{\partial t} = R_{sn} \left(1. - F(h_{w1}) \right) - Q_{ns} + \dot{wf} \rho_w \left[L_w + c_w \left(T_{w1} - T_{0°C} \right) \right] - \rho_w c_w k_{w1} \frac{T_{w1} - T_{w2}}{z_1 - z_2} \tag{11}$$

where

$$Q_{ns} = -R_{ld} + \sigma T_s^4 + H + LE - rain\,\rho_w[c_w(T_{rain} - T_{w1})] - snowfl\,\rho_w[c_{sn}(T_{snowfl} - T_{0°C}) - L_w + c_w(T_{0°C} - T_{w1})] - im\,\rho_w[c_w(T_{0°C} - T_{w1})] - infl\,\rho_w[c_w(T_{in} - T_{w1})] \quad (12)$$

Note that we assume the outflow temperature from the lake is T_{w1}. Therefore, the advected energy of outflow is zero. In addition, in the model, T_{rain} and T_{snowfl} are assumed to be equal to surface air temperature at 2 m height, and T_{in} is also assumed to be T_{w1}.

The mass conservation equation for the uppermost layer of water is determined as:

$$\frac{\partial h_{w1}}{\partial t} = snowfl + rain + inf\,l + u_{iw} - icf - E \quad (13)$$

where $inf\,l$ is river discharge rate runoff (m s^{-1}) and E is evaporation rate (m s^{-1}).

2.2.4. Metaphorism (Phase Change) at the Surfaces:

The snow melting rate, ice melting rate and water freezing rate are three extra variables needed equations to determine. The melting and freezing always occur at the surface of a snow, ice or water pack while its surface temperature is 0℃. They are determined by calculating potential skin temperatures of these surfaces. If the potential skin temperature of either a snow pack or an ice pack is higher than zero degree Celsius, then there is extra energy for melting. If the potential skin temperature of water is less than zero degree Celsius, then freezing occurs. The potential skin temperature of snow T_{sn0}^* is determined as:

$$\rho_{sn} c_{sn} h_{esn} \frac{\partial T_{sn0}^*}{\partial t} = R_{sn} - Q_{ns} - \rho_{sn} c_{sn} k_{sn} \frac{T_{sn0}^* - T_{sn1}}{h_{sn}/2} \quad (14)$$

where

$$h_{esn} = \sqrt{\frac{k_{sn}}{\omega}}\left(1 - \exp\left(-\frac{h_{sn}/4}{\sqrt{2k_{sn}}}\right)\right) \quad (15)$$

If the calculated T_{sn0}^* is large than $T_{0°C}$, snow melts at the surface. Then, set $T_{sn0} = T_{0°C}$. The remaining energy is used to melt snow. The phase change energy at

the snow surface is:

$$FCE = -\rho_{sn} c_{sn} h_{esn} (T_{0°c} - T_{sn0}) + \Delta t \left(R_{sn} - Q_{ns} - \rho_{sn} c_{sn} k_{sn} \frac{T_{sn0} - T_{sn1}}{h_{sn}/2} \right) \tag{16}$$

FCE should be positive. The amount of melted snow equals to:

$$sm = Min\left[\frac{FCE}{\rho_w (L_w + c_{sn}(T_{o°C} - T_{sn1}))}, sn \right] \tag{17}$$

If sm equals sn, snow melts completely. Otherwise, put the above equation into (1). We can rewrite equation (1) as:

$$\frac{\partial T_{sn1}}{\partial t} = \frac{h_{esn}(T_{0°c} - T_{sn0})}{h_{sn}\Delta t} + \frac{wfs\,\rho_w [L_w + c_{sn}(T_{0°C} - T_{sn1})]}{\rho_{sn} c_{sn} h_{sn}} + k_{sn} \frac{T_{sn0} - T_{sn1}}{h_{sn}^2/2} - k_{sn} \frac{T_{sn1} - T_{i0}}{h_{sn}^2/2} \tag{1b}$$

A general equation valid at both melting stage and non-melting stage is written as:

$$\frac{\partial T_{sn1}}{\partial t} = \frac{h_{esn}}{h_{sn}} \frac{\partial T_{sn0}}{\partial t} + \frac{wfs\,\rho_w [L_w + c_{sn}(T_{0°C} - T_{sn1})]}{\rho_{sn} c_{sn} h_{sn}} + \frac{\partial}{\partial z} k_{sn} \frac{\partial T_{sn1}}{\partial z} \tag{1c}$$

or

$$\frac{\partial T_{sn1}}{\partial t} = \frac{h_{esn}}{h_{sn}} \frac{\partial T_{sn0}}{\partial t} + \frac{Q_{sn}}{\rho_{sn} c_{sn} h_{sn}} + \frac{\partial}{\partial z} k_{sn} \frac{\partial T_{sn1}}{\partial z} \tag{1d}$$

where Q_{sn} is the energy production rate in the snow pack that is not counted by the increase of skin temperature (w m^{-2}). It equals:

$$Q_{sn} = wfs\,\rho_w [L_w + c_{sn}(T_{0°C} - T_{sn1})] \tag{18}$$

at this case. Note that we assume liquid water refreeze inside the snow pack, not on the surface.

$$CG_{sn} \frac{\partial PST_{sn}}{\partial t} = (1 - \alpha_{sn}) R_s - R_{ld} - \sigma T_{sn}^4 - H - LE + snowfl\,\rho_w [c_w (T_{snowfl} - T_{sn})] + rain\,\rho_w [c_w (T_{rain} - T_{0°C})] + Q_{snss} \tag{19a}$$

$$CG_{si} \frac{\partial PST_{si}}{\partial t} = -\delta_{sn} Q_{sisn} + (1 - \delta_{sn}) \left\{ (1 - \alpha_{ice}) R_s - R_{ld} - \sigma T_{sice}^4 - H - LE + rain\,\rho_w [c_w (T_{rain} - T_{0°C})] \right\} + Q_{icesi} + \frac{1}{r_{ic}} \left[\left(wfs + wfi \right) \rho_w [L_w + c_w (T_{0°C} - T_{ice})] + Q_{rsn} \right] \tag{19b}$$

$$CG_{iw}\frac{\partial PST_{iw}}{\partial t} = -Q_{iwice} + Q_{w1iw} + \frac{1}{r_{ic}}\left[im\,\rho_w\left[c_w\left(T_{0°C} - T_{w1}\right)\right] + wf\,\rho_w\left[L_w + c_w\left(T_{w1} - T_{ice}\right)\right] + Q_{rice}\right] \quad (19c)$$

$$CG_w\frac{\partial PST_w}{\partial t} = \left(1-\alpha_w\right)R_s\left[F(0) - F\left(h_1/4\right)\right] + R_{ld} - \sigma T_{sw}^4 - H - LE + snowfl\,\rho_w\left[-L_w + c_w\left(T_{snowfl} - T_{w1}\right)\right] + rain\,\rho_w\left[c_w\left(T_{rain} - T_{w1}\right)\right] + Q_{w1ws} \quad (19d)$$

where PST_{sn} is the potential skin temperature of snow. PST_{si} is the potential skin temperature of snow and ice interface, and if there is no snow, it's the skin temperature of ice. PST_{iw} is the potential skin temperature of ice and water interface. PST_w is the potential skin temperature of water. CG is the unit area heat capacity of snow surface, ice surface, ice-water interface and water surface. They can be expressed as :

$$CG_{sn} = \rho_{sn}c_{sn}\sqrt{\frac{k_{sn}}{\omega}}\left(1 - \exp\left(-\frac{h_{sn}/4}{\sqrt{2k_{sn}}}\right)\right) \quad (20a)$$

$$CG_{si} = \delta_{sn}\left(\rho_{sn}c_{sn}h_{sn}/4 + \rho_{ice}c_{ice}h_{ice}/4\right) + \left(1-\delta_{sn}\right)\rho_{ice}c_{ice}\sqrt{\frac{k_{ice}}{\omega}}\left(1 - \exp\left(-\frac{h_{ice}/4}{\sqrt{2k_{ice}}}\right)\right) \quad (20b)$$

$$CG_{iw} = \rho_{ice}c_{ice}h_{ice}/4 + \rho_w c_w h_{w1}/4 \quad (20c)$$

$$CG_w = \rho_w c_w\sqrt{\frac{k_{w0}}{\omega}}\left(1 - \exp\left(-\frac{h_{w1}/2}{\sqrt{2k_{w0}}}\right)\right) \quad (20d)$$

If the calculated PST_{sn} is higher than 0 degree C, snow melts. If the PST_{si} is higher than 0 degree C, snow melts first, but if there is no snow left, ice starts to melt. If the PST_{iw} is higher than 0 degree C, ice melts, and if it is less 0 degree C, water freezes. If the PST_w is less than zero degree Celsius, water freezes.

2.2.5. Melting & Freezing rate:

Melting rate of snow (*sm*), of ice (*im*), freezing rate of snow (*wfs*), of ice (*wfi*) and of water (*wf*) can be expressed as:

$$sm = Min\left[\frac{CG_{sn}Max\left(PST_{sn} - T_{o°C}, 0\right)}{\rho_w\left(L_w + c_w\left(T_{o°C} - T_{sn}\right)\right)}, sn\right] \quad (21a)$$

$$wfs = Min\left[\frac{CG_{sn}Max(T_{o°C} - PST_{sn},0)}{\rho_w(L_w)}, wsn\right] \tag{21b}$$

$$im = Min\left[\frac{CG_{ice}Max(PST_{ice} - T_{o°C},0)}{\rho_w(L_w + c_w(T_{o°C} - T_{ice}))}, ice\right] \tag{21c}$$

$$wfi = Min\left[\frac{CG_{ice}Max(T_{o°C} - PST_{ice},0)}{\rho_w(L_w)}, wice\right] \tag{21d}$$

$$wf = \frac{CG_wMax(T_{o°C} - PST_w,0)}{\rho_w(L_w + c_w(T_{w1} - T_{0°C}))} \tag{21f}$$

where

$$CG_i = \rho_i c_i \sqrt{\frac{k_i}{\omega}}\left(1 - \exp\left(-\frac{2h_i}{\sqrt{2k_i/\omega}}\right)\right) \tag{22}$$

$$\frac{\partial PST_i}{\partial t} = \frac{1}{CG_i}\left[Q_s + Q_{hi}\exp\left(-\frac{h_i}{\sqrt{2k_i/\omega}}\right)\right] \tag{23}$$

where Q_s = heat flux into the skin. Q_{hi} = heat flux at distance h_i apart from skin surface (positive toward the skin).

2.2.6. Thermocline

Lake parameterization for climatic models can borrow experiences from ocean modeling. Lakes in comparison with oceans are smaller and shallower. As a consequence, advection terms in lakes are not as important. The advection terms are neglected in parameterization. Traditionally, there are two approaches to simulate the thermocline of a water body: a bulk mixed layer approach and an eddy kinetic energy approach. The eddy kinetic energy approach is time consuming. Hostetler et al. (19??) discretize the entire water column into 1 m thickness, Gaspar et al. (1990) used a vertical resolution of 1 m from the surface down to 30 m, and Martin (1985) chose a vertical resolution of 2 m at the surface and 13 m at 100-m depth. On the other hand, the bulk mixed layer approach (Niller, 1975; Davis et al., 1981; Garwood, 1977; Garwood, 1985a; 1985b) is simple and computationally efficient, and has been used and tuned into global ocean models (Wells, 1979; Admamec et al., 1981; Schopf and Cane, 1983; Oberhuber, 1993). However, it suffers a major assumption that the eddy diffusivity is infinity in the mixed layer. Therefore, an input of mass, energy and momentum at any location in the mixed layer will redistribute to the entire mixed

layer in an infinite small time step. As a consequence, the seasonal and especially the diurnal variations of the surface temperature, salinity and velocities due to surface heating, evaporation and precipitation, and wind shear might be underestimated. Nonetheless, accurate determination of these properties at the surface is important for energy, mass and momentum exchange between a water body and the atmosphere. On the other hand, although the eddy kinetic energy approach determines a more realistic diurnal variation (Hostetler et al., 19??; Gaspar et al., 1990), most schemes assume the temperature in the first layer from the surface is the skin temperature. It in fact is the temperature at the depth of half of the thickness of the numerical first layer, with a depth of 0.5 m in Gaspar et al. (1990). Gaspar et al. found a 0.5-m vertical resolution improves the result, and a 5-m resolution appeared to be insufficient to resolve the strongly surface trapped response of the upper ocean where the large diurnal cycles of the SST are poorly simulated. Their maximum amplitude is reduced to a few tenths of a degree, while the observation is around 1 degree. To overcome the drawback, this study introduces a skin layer to simulate the skin temperature (Tsuang, in revision).

Although parameterization for a lake is easier than for the ocean, one has to have in mind that nearby land also influences the wind profiles above a lake. Hence, equations to determine the exchange coefficients between a lake and the atmosphere are different from oceans. Special attention has to be taken to determine these coefficients.

2.2.6.1. Governing Equations

(a) Staggered Grid:

$$\frac{\partial \overline{T}}{\partial t} = \frac{R_{sn}}{\rho_0 c_p}\frac{\partial F}{\partial \tilde{z}} - \frac{\partial \overline{T'w'}}{\partial \tilde{z}} \tag{24}$$

$$\frac{\partial \overline{S}}{\partial t} = -\frac{\partial \overline{S'w'}}{\partial \tilde{z}} \tag{25}$$

$$\frac{\partial \overline{U}}{\partial t} = -\frac{\partial \overline{U'w'}}{\partial \tilde{z}} \tag{26}$$

(b) At the center of a grid:

$$\overline{T'w'} = -k_E \partial \overline{T} / \partial \tilde{z} \tag{27a}$$

$$\overline{S'w'} = -k_E \partial \overline{S} / \partial \tilde{z} \tag{27b}$$

$$\overline{U'w'} = -k_E \partial \overline{U} / \partial \tilde{z} \tag{27c}$$

$$\frac{\partial \overline{E}}{\partial t} = \frac{\partial}{\partial \overline{z}} k_E \frac{\partial \overline{E}}{\partial \overline{z}} + k_E \left(\frac{\partial \overline{U}}{\partial \overline{z}} \right)^2 + k_E \frac{g}{\rho_0} \frac{\partial \overline{\rho}}{\partial \overline{z}} - c_\varepsilon \frac{\overline{E}^{3/2}}{l_\varepsilon} \tag{28}$$

(c) At boundaries of a grid:

$$k_E = c_k l_k \sqrt{\overline{E}} \tag{27}$$

$$\rho = \rho(T, S) \tag{28}$$

$$l_\varepsilon = \sqrt{l_u l_d} \tag{29}$$

$$l_k = \min(l_u, l_d) \tag{30}$$

$$\frac{g}{\rho_0} \int_z^{z+l_u} \overline{\rho}(z) - \overline{\rho}(z') dz' = \overline{E}(z) \tag{31a}$$

$$\frac{g}{\rho_0} \int_z^{z-l_d} \overline{\rho}(z) - \overline{\rho}(z') dz' = \overline{E}(z) \tag{31b}$$

$$F = re^{z/\xi_1} + (1-r)e^{z/\xi_2} \tag{32}$$

$$\frac{\partial F}{\partial z} = \frac{r}{\xi_1} e^{z/\xi_1} + \frac{(1-r)}{\xi_2} e^{z/\xi_2} \tag{33}$$

where c_k = 0.1 (ocean) (Gaspar et al., 1990), $c_\varepsilon = 0.7$ (atmosphere) (Bougeault and Lacarrere, 1989). For Jerlov Type I water: $\xi_1 = 0.35m$, $\xi_2 = 23m$, and r = 0.58.

$$\frac{\partial F(0)}{\partial z} = \frac{r}{\xi_1} + \frac{(1-r)}{\xi_2} = 1.68m^{-1} \tag{34}$$

2.2.6.2. Boundary Condition:

$$\overline{T'w'}(0) = (R_{lu} - R_{ld} + H + LE)/\rho_0 c_p \tag{35}$$

$$\overline{S'w'}(0) = -\left(E_{vap} - ppt - infl \right) \overline{S}(0) \tag{36}$$

$$\overline{U'w'}(0) = -\tau/\rho_0 = -u_*^2 \tag{37}$$

$$\overline{E}(0) = \overline{E}_0 = \overline{E}_1 \tag{38}$$

$$\overline{T'w'}(-d) = -k_E \frac{\overline{T}_n - \overline{T}_g}{z_n - z_g} \tag{39}$$

$$\overline{S'w'}(-d) = 0 \tag{40}$$

$$\overline{U}(-d)=0 \tag{41}$$

$$\overline{E}(-d)=\overline{E}_n=\overline{E}_{n-1} \tag{42}$$

where "*0* " means the condition at surface, and "*-d* " means the condition at the bottom of the lake point.

2.3. Advection

A simple advection term was added to the lake routine (Figure 4) (lakeadv.f90). The subroutine first calculates the mean water level of the entire lake. Then, it locates surplus lake grids and deficit lake grids. Then, it calculates the mean u-current, v-current, water temperature, salinity and turbulent kinetic energy (*u*, *v*, *T*, *S* and TKE) of surplus water. Finally, it puts the surplus water to the top layers of deficit grids and recalculates the mean properties (*u*, *v*, *T*, *S* and TKE) of the top layers of the deficit lake grids. The current lake routine does not have a horizontal diffusion term.

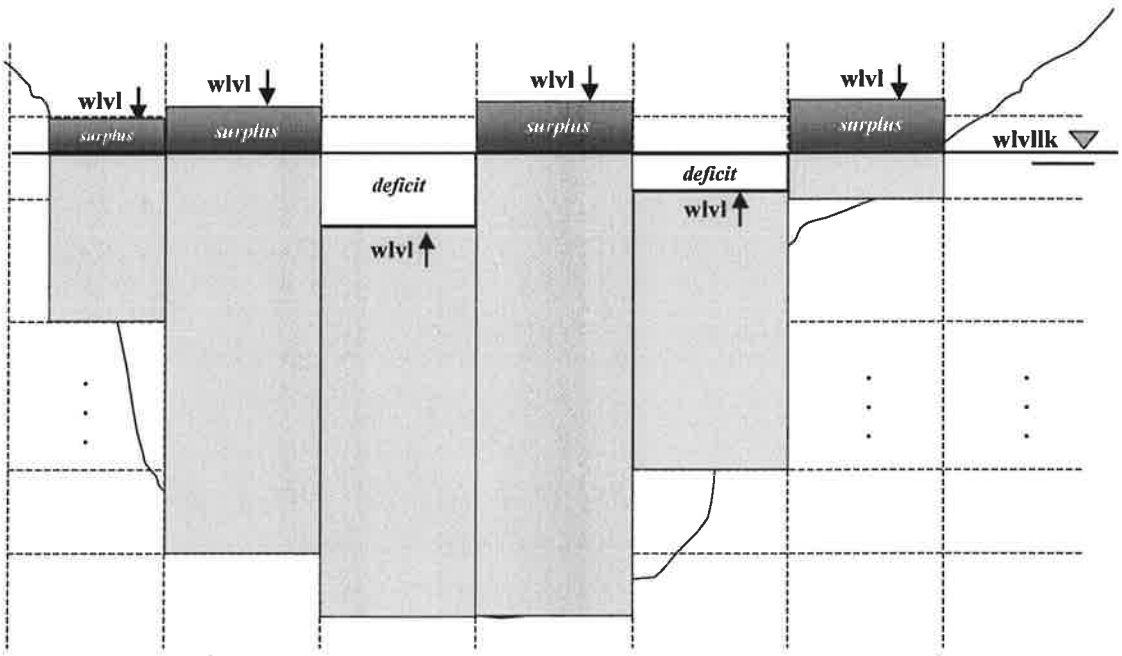

Figure 4 Schematic of advection algorithm of the lake routine.

2.4. Albedo and Roughness

The couple run does not change the code for determining roughness and albedo in ECHAM. ECHAM determines albedo according to land-sea mask and the existence of ice. The albedo over sea is about 0.07. If the routine produces ice over water, the albedo of the grid will change to the value for ice (0.5-0.75) (function of temperature) (Robock, 1980). However, ECHAM does not change the value of albedo to snow (~ 0.8) if there is snowfall over ice (see the subroutine "radint.f90"). ECHAM calculate roughness over sea by using Charnock's formula (Miller et al., 1992). If there is ice, the roughness will change to the value for sea ice (0.01m) (see the subroutine "vdiff.f90").

2.5. Initialization

2.5.1. Theory

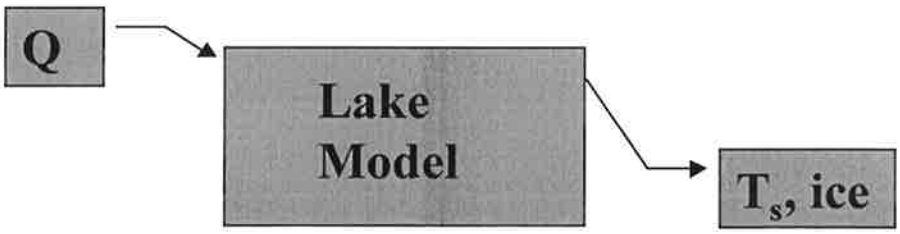

Figure 5 schematic of energy pumping.

A technique of energy pumping is used for initialization as shown in Figure 5. Since the water temperature has a long memory on its initial value, we have to determine its initial temperature profile carefully. However, we are not able to obtain temperature profiles globally. A technique of energy pumping is used for initialization. Since we can obtain sea surface temperature from satellite, the no-solar energy Q can be determined by an energy pumping technique. The energy pumping technique determines non-solar energy Q by trial-and-error to minimize the error between calculated-and-observed skin temperature. There exists a utility function $P(Q)$ as:

$$P(Q)=\rho_c c_c\sqrt{\frac{k_c}{\omega}}(T_c-T_{0^\circ C})+\rho_o c_o\sqrt{\frac{k_o}{\omega}}(T_{0^\circ C}-T_o)-\rho_w L_f(ice_c-ice_o) \qquad (43)$$

If Q is the non-solar energy, the calculated skin temperature should equal to the observed temperature, i.e. $P(Q)=0$. If there is difference between calculated and observed skin temperature, according to the Newton method, Q converges to:

$$Q_{n+1} = Q_n - \frac{P(Q_n)}{\partial P / \partial Q} \tag{44}$$

or we can use a bi-section method to solve the above utility function.

2.5.2. Energy Pumping

Monthly net radiation, precipitation, snowfall, evaporation, wind stress and annual mean Volga river inflow are used as inputs for the energy pumping over the Caspian Sea. To prevent undesired water level change, water levels are set to be –28 m after the simulation of each month. The pumping starts from January 1980 and ends in February 1994.

Figure 6 shows the 14-year mean (1980-1993) of net energy budget over the Caspian Sea from ECMWF reanalysis data set. It shows that the net energy flux was not balanced over the Caspian Sea (not zero), but the flux was balanced (becomes zero) over land grids. This implies the energy budget is not closed over the Caspian Sea. Using a prescribed SST in the ECMWF reanalysis caused the unbalanced energy budget.

The results (not shown here) of comparing skin temperature and net heat flux between data obtained from ECMWF reanalysis and the results of the energy pumping shows that over lake grids the skin temperatures obtained by the energy pumping are almost identical to the ECMWF reanalysis data set. Their difference is less than 1 K. But significant difference was found in net heat flux. The pumping technique obtains upward heat flux in February and downward net heat flux in August, especially at locations where the lake is deep (South). However, the reanalysis data set does not shows significant variations between the north and the south. The neglection of horizontal advection and diffusion terms in the lake routine may contribute to the difference.

Figure 7 shows a comparison of the 5-year mean (1989-1993) of net energy budget over the Caspian Sea from ECMWF reanalysis data set and the results of the energy pumping. The 5-year mean net heat flux from ECMWF reanalysis data set is similar to 14-year mean net heat flux as shown in Figure 6. That means the net energy flux was not balanced over the Caspian Sea (-20 W m^{-2} ~ 60 W m^{-2}). On the other hand, the net heat flux simulated by the energy pumping was balanced (-20 W m^{-2} ~ 10 W m^{-2}).

Figure 8 shows the simulated profiles of water temperature, salinity, current, heat diffusivity, turbulent kinetic energy, mixing length from April 1991 – April 1993 at a southern grid (38.648° N, 51.1875° E) of the Caspian Sea by the energy pumping. It shows there is a spring turnover (February- March) at the grid, and the thermocline

stratified from April to January. The hottest SST was in August and the coldest was in February. Salinity stratification from June to January was also simulated. During the turnover periods, the heat diffusivity, turbulent kinetic energy and mixing length were much larger than in the stratification periods.

Figure 9 and 10 shows the simulated N-S cross-section of profiles of water temperature, salinity, current, heat diffusivity, turbulent kinetic energy, mixing length in February 1992 and August 1992 at 51.1875E, respectively. It shows that the thermal structure was reasonable, but it was too salty at the most northern grid of the Caspian Sea. If the net fresh water inflow (ppt –Evap+Infl) is not balanced, there will be a trend in the time series of salinity. At the northern grids of the Caspian Sea, the water was very shallow. Hence, salinity would change dramatically due to the imbalance of fresh water inflow.

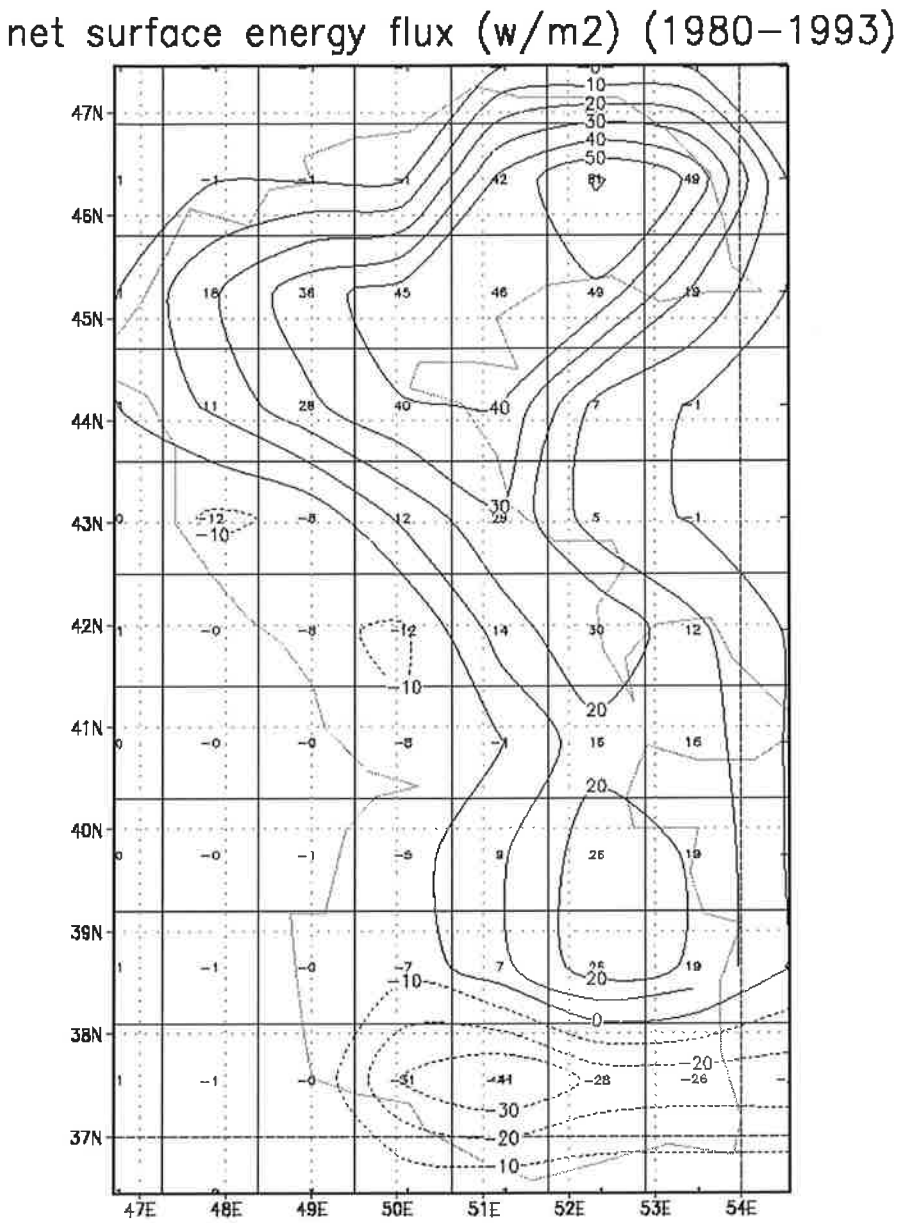

Figure 6 ECMWF-14 year mean (1980-1993) of net energy budget over the Caspian Sea .

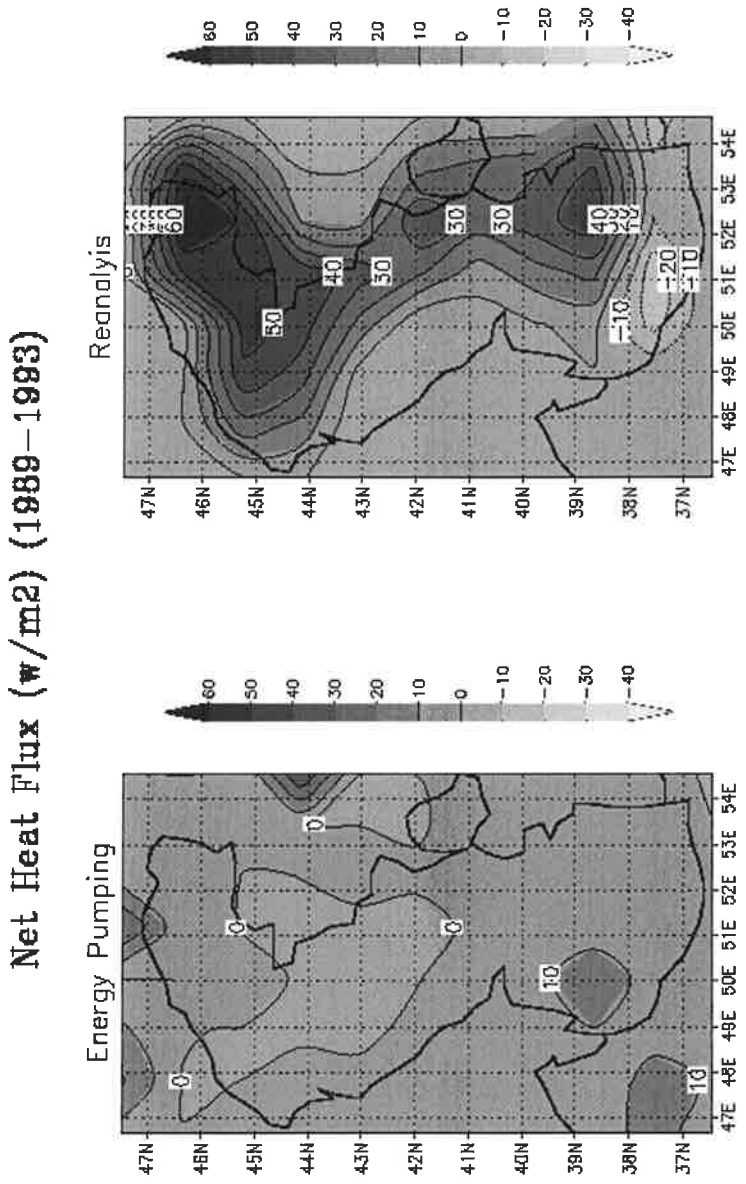

Figure 7 A comparison of 5-year mean (1989-1993) net heat between data obtained from ECMWF reanalysis and the results of the energy pumping.

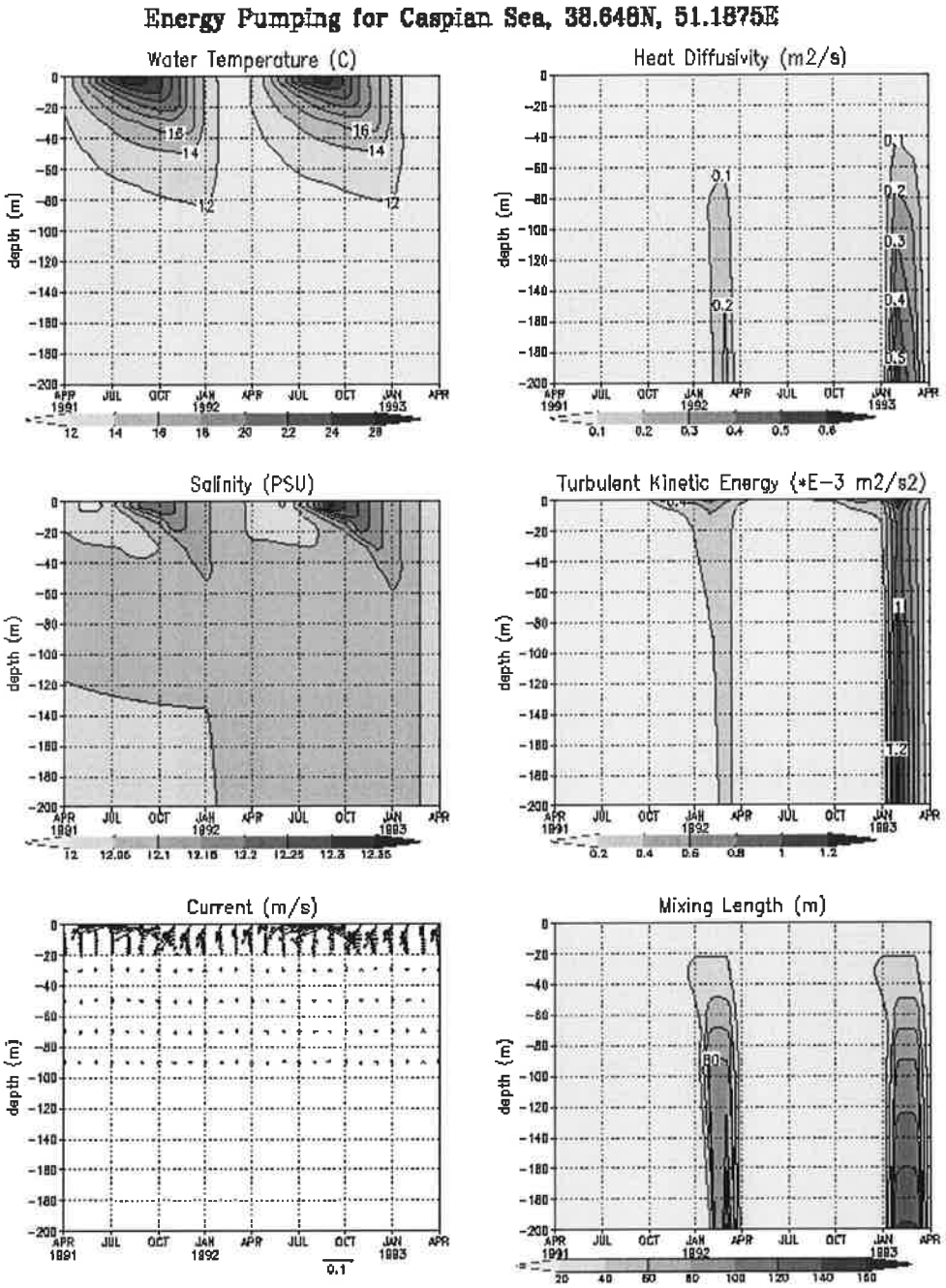

Figure 8 Simulated profiles of water temperature, salinity, current, heat diffusivity, turbulent kinetic energy, mixing length from April 1991 – April 1993 at a southern grid (38.648 N, 51.1875E) of the Caspian Sea by the energy pumping.

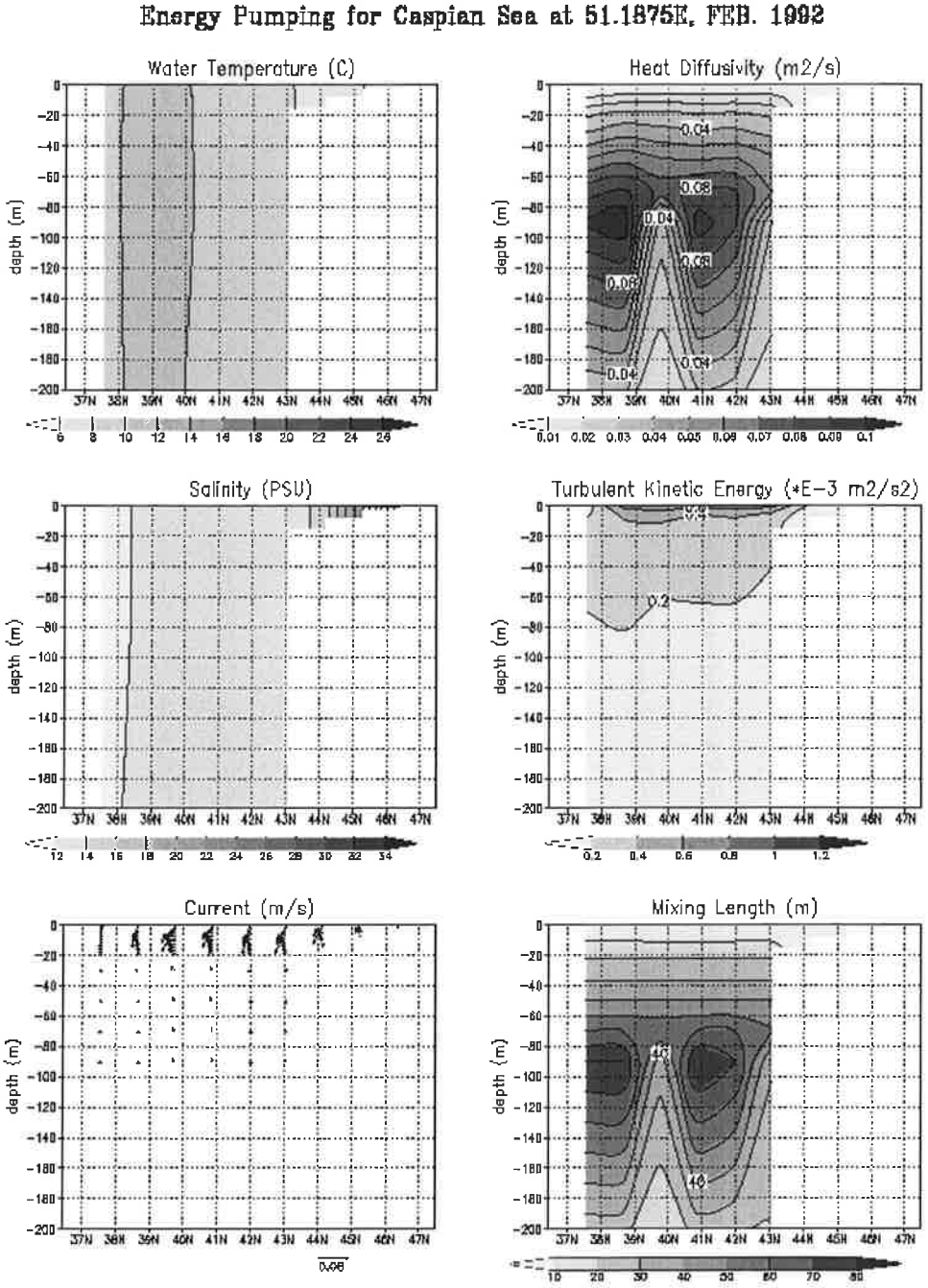

Figure 9 Simulated x-sliced profiles of water temperature, salinity, current, heat diffusivity, turbulent kinetic energy, mixing length in February 1992 at 51.1875E.

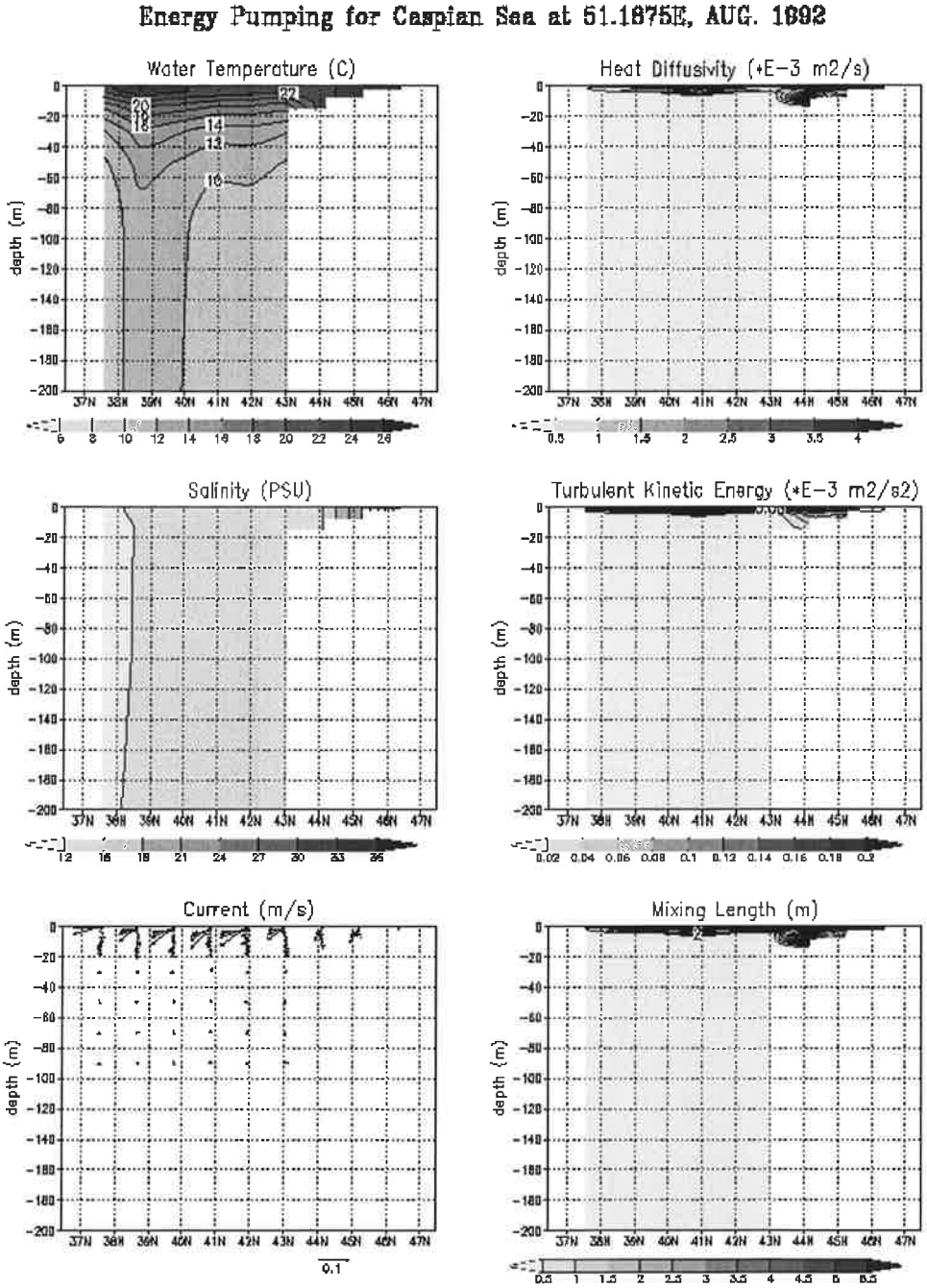

Figure 10 Simulated x-sliced profiles of water temperature, salinity, current, heat diffusivity, turbulent kinetic energy, mixing length in August 1992 at 51.1875E.

3. System Description

3.1. Input Data Set

3.1.1. Overview

The initial profiles of thermocline, salinity, current and turbulent kinetic energy of each lake grids were derived by energy pumping. There is no salinity flux used for the pumping to prevent undesired salinity profiles as shown in the previous section. In addition, to prevent undesired water level change, an artificial fresh water flux $\Delta Infl$ (m yr^{-1}) was added to each grid as:

$$\Delta Infl = \frac{wlvlref - wlvl}{year} \tag{45}$$

Note that if there is no water level correction, the simulated water level of the Caspian Sea will increase 1.8 m per year as shown in a test run (h92001).

Two data set are needed to drive the lake routine. One is information of lakes (lake(lkp)%……). The other is information of each lake grid (lakegd(lkp)%……). Of each lake, the model needs its 1) name or ID (name), 2) its maximum depth (dpthmx), 3) its outlet's elevation (elvmx), 4) its reference water level (wlvlref) and 5) its current water level (wlvllk). For each lake grid, the model needs: 1) its lake ID (lkid), 2) latitude id in the Gaussian grid (lat), 3) irow in the Gaussian grid (irow), 4) longitude id in the Gaussian grid (ilon), 5) elevation of lake bed (topo), 6) lake water fraction in the Gaussian grid (wf), 7) initial vertical profiles of u, v, T, S, TKE of each lake grids and 8) monthly surface river discharge rate (inflow). These information are stored in module "mo_lake.f90". The initial vertical profiles of u, v, T, S can be derived from energy pumping technique as shown in the previous section. Then, surface SST, surface salinity, solar radiation, wind shear stress, precipitation, evaporation are needed to drive the energy pumping routine (ECMWF reanalysis data set were used in this study).

3.1.2. Preparation

There are 4 steps to prepare the input data set.

Step1: There are two parts in this step. First part convert bathymeter and water fraction of terrain from 0.5° x 0.5° to T42 or T106. The second part convert 1° x 1° runoff data from Samuel's & Cox's GFDL Global Oceanographic Data Set Atlas to T42 or T106. River discharge for the Caspian Sea and the Great Lakes

are additional added to the correspondent grids.

Step2: First assign basic information (LAKEINFO) to each lake grids. LAKEINFO includes latitude, longitude and name of the lakes. Then read data from the output files of step1. All the parameters in module mo_lake are assigned in this step.

Step3: This is the step for energy pumping. 1st run is the cold run and pump with cold start by reading from the output data files of step2. 2nd run is the climate run and pump by reading from the output data files of 1st run. 3rd run is the normal run and pump by reading from the output data files of 2nd run. ECMWF reanalysis data set are used in step2 and step3.

Step4: The big lakes subscribed in step1~step3 include Hudson Bay (H), Baltic Sea (B), Great Lake (X), Black Sea (S), Caspian Sea (C), Persian Gulf (G) and Red Sea (R). This step picks out the big lakes that will be calculated with lake routine, also determines the initial date of the ECHAM run.

Step4 produces 3 files, "lake.dir", "lakegd.dir" and for example 42lake197901.XC ("42" means T42, "197901" means starting month and "XC" means the Great Lakes and the Caspian Sea will be calculated.). "lake.dir" and "lakegd.dir" describe the basic information of the lakes and the lake grids that will be calculated.

3.2. Coupled with ECHAM-4

The one-column lake routine was coupled with ECHAM-4 in T42 resolution (DKRZ, 1994; Roeckner et al., 1996). Only eight T42 grids were simulated by the lake routine. There are 6 grids for the Caspian Sea and 2 grids for the Great Lakes. The AMIP SST data set (Gates, 1992) was used to drive the model. The simulation starts from October 1981 and continues until December 1993. The run of the lake routine coupled with ECHAM-4 is discussed in later section.

3.3. Coupled with ECHAM-5

3.3.1. General

The main difference of the surface process between ECHAM-4 and ECHAM-5 is the consideration of different surface covers. In ECHAM-5 each resolution grid is combined with partial land and partial water, which in ECHAM-4 is treated as

homogeneous. With T42 resolution in ECHAM-4 only 6 grids for the Caspian Sea and 2 grids for the Great Lakes were simulated by the thermocline lake routine (hereafter denoted as "THMLAKE"). It becomes 10 grids for the Caspian Sea and 13 grids for the Great Lakes with the same resolution in ECHAM-5. But due to the availability in ECMWF data set, only 8 grids for the Caspian Sea and 5 grids for the Great Lakes are considered. Moreover, the lake water fraction (wf) in each grid has to be considered when dealing the advection between different lake grids in ECHAM-5.

Due to the consideration of partial water in the grids, there are 550 lake grids in the T42 land-sea mask. For computing efficiency, not all of the 550 grids are calculated by the THMLAKE, but only the big lakes. Instead a simple lake routine (hereafter denoted as " LAKE") considering only surface energy budget for lake surface water and ice temperatures is applied in ECHAM-5. The logical variable "Lthmlake" determines whether the THMLAKE is turned on or not. The logical variable "Lbiglake" determines whether the grid is a big lake to be calculated with THMLAKE or a small lake to be calculated with LAKE.

The big lakes subscribed in step1~step3 include Hudson Bay (H), Baltic Sea (B), Great Lake (X), Black Sea (S), Caspian Sea (C), Persian Gulf (G) and Red Sea (R). Because the coupled atmosphere-ocean model ignore the existence of the Caspian Sea and the Great Lakes completely, the THMLAKE coupled with ECHAM-5 considers only the Caspian Sea and the Great Lakes.

3.3.2. Flow Diagram

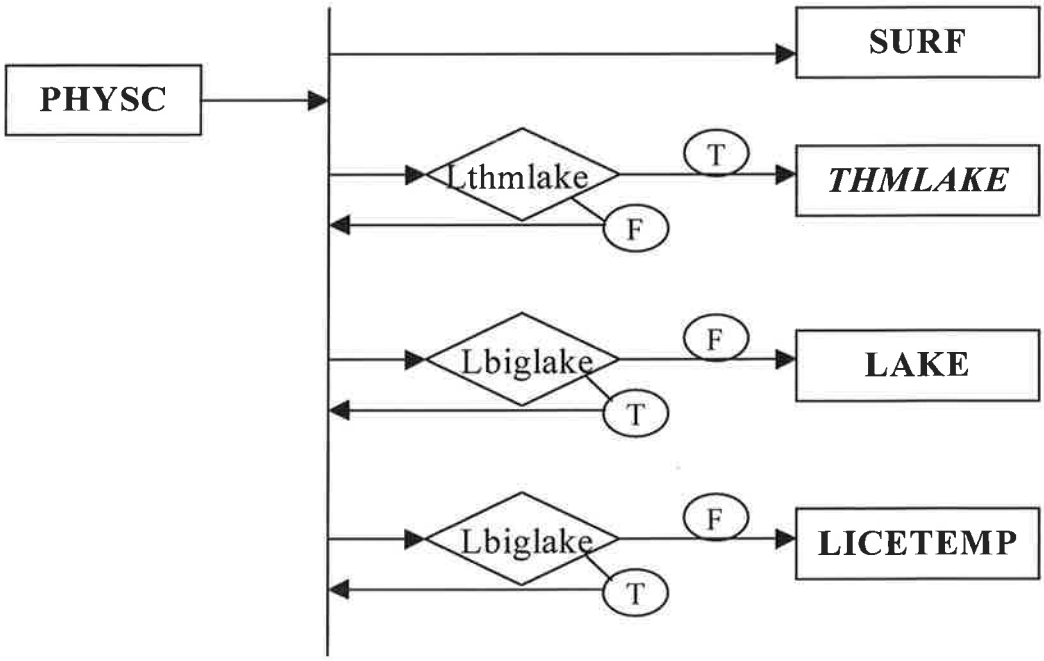

Figure 11 Flow diagram showing the role of the THMLAKE in subroutine PHYSC.

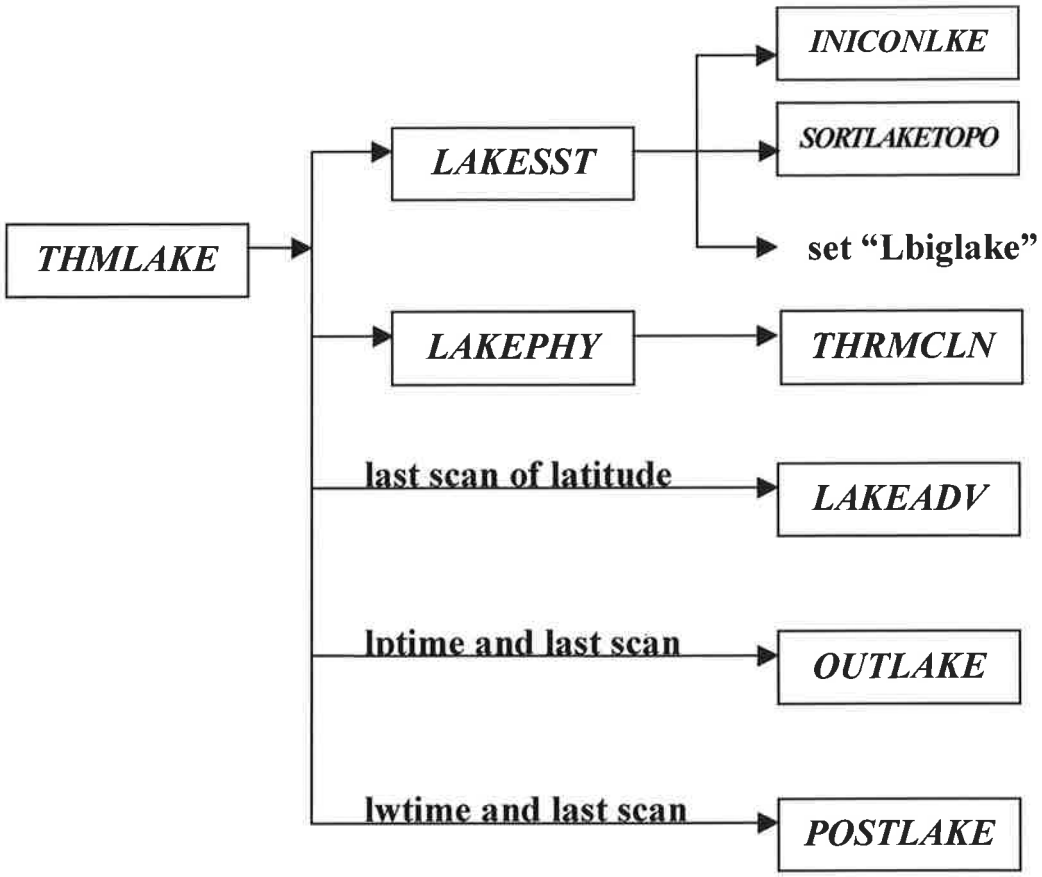

Figure 12 Flow diagram showing the detailed structure of the thermocline lake computation, which is controlled by the subroutine THMLAKE.

3.3.3. Subroutines in Alphabetical Order

The list of called routines by the THMLAKE consists of:

ALLOC_LAKE allocates prognostic variables storage. It is described in "lakesst.f90", and called in INILAKE and RESLAKE.

ALLOC_LAKEEXT allocates prognostic variables storage. It is described in "lakesst.f90", and called in INILAKE, RESLAKE and LAKESST

CALCWLVL calculates the water level of each big lake. It is described in "lakeadv.f90", and called in LAKEADV.

EDDY computes eddy mixing coefficients. It is described in "thmcln.f90", and called in THMCLN.

LKCORD determines the coordinates of each lake point. It is described in "mo_lake.f90", and called in PZCORD.

LKDIFKH	computes eddy mixing coefficient matrix for temperature and salinity. It is described in "thmcln.f90", and called in THMCLN.
LKDIFKM	computes eddy mixing coefficient matrix for TKE. It is described in "thmcln.f90", and called in THMCLN.
LKERR	writes error message to "lake.message". It is described in "thmcln.f90", and called in THMCLN.
LU prepares	the coefficients of the tridiagonal matrix for temperature and salinity. It is described in "thmcln.f90", and called in THMCLN.
LU2 prepares	the coefficients of the complex tridiagonal matrix for TKE. It is described in "thmcln.f90", and called in THMCLN.
ICOMP_XCHG	is for the index of bathymeter sorting. It is described in "sortlaketopo.f90", and called in SORTLAKETOPO.
INDEXX	is the index of bathymeter sorting for all the lake grids. It is described in "sortlaketopo.f90", and called in SORTLAKETOPO.
INICONLKE	sets constants used in the THMLAKE. It is described in "mo_lake.f90", and called in LAKESST
INILAKE	allocates the prognostic variables storage and reads initial values for prognostic variables from input file. It is described in "lakesst.f90", and called in LAKESST.
LAKEADV	is turned on when the computation of all the lake grids is finished. It is described in "lakeadv.f90", and called in the THMLAKE.
LAKEPHY	calculates net surface energy flux for THMCLN. It is described in "lakephy.f90", and called in the THMLAKE.
LAKESST	determines the grids of big lakes (Lbiglake). It also allocates the prognostic storage and sets prognostic variables. It is described in "lakesst.f90", and called in the THMLAKE.
OUTLAKE	writes the THMLAKE data to output file when the write-up time is due. It is described in "mo_outlake.f90", and called in the THMLAKE.

POSTLAKE	writes the THMLAKE data to rerun files before the run is interrupted. It is described in "mo_outlake.f90", and called in the THMLAKE.
PZCORD	determines the coordinates of each lake point. It is described in "mo_lake.f90", and called in LAKEADV.
RESLAKE	allocates the prognostic variables storage and reads initial values for prognostic variables from rerun file. It is described in "lakesst.f90", and called in LAKESST.
SORTLAKETOPO	sorts lake grids according to the bathymeter of the terrain. It is described in "sortlaketopo.f90", and called in LAKESST.
SWAP	is for the index of bathymeter sorting. It is described in "sortlaketopo.f90", and called in SORTLAKETOPO.
THMCLN	is for the computing of thermocline scheme. It is described in "thmcln.f90", and called in LAKEPHY.

3.3.4. Module Files

Two module files are prepared for the THMLAKE. One is module "mo_lake", the other one is module "mo_outlake". Module "mo_lake" prepares 4 types of variables to store lake and lake grid information. The type "laketype" and "lakeexttype", which are allocated as "lake(:)" and "lakeext(:)" in subroutines, store basic information of each lake. The type "lakegridtype" and "lakegridexttype", which are allocated as "lakegd (:)" and "lakegdext (:)" in subroutines, store basic information of each lake grid. Module "mo_lake" also contains subroutines INICONLKE, LKCORD, PZCORD and function LKEPTR. Module "mo_outlake" is for writing variables to the THMLAKE output file and rerun file. It contains subroutines the POSTLAKE and the OUTLAKE.

3.3.5. I/O

The input and output files for the THMLAKE are designated in "mo_start-dataset.f90".

3.3.5.1. New Start

Subroutine INILAKE reads from the initial file for the THMLAKE only when

the simulation starts in the very beginning. The file is assigned to unit.71 (nilk). Step4 of energy pumping in the previous section prepares this file. If the starting month of the ECHAM-5+Thnlake is changed, one must submit Step4 again to have the new file with the same starting time with ECHAM-5+THMLAKE.

3.3.5.2. Rerun

Subroutine RESLAKE reads from the rerun file for the THMLAKE when the simulation restarts. The frequency of the rerun file write-up is determined by the logical variable "Lptime", which is described in the shell script for running ECHAM-5. The file is assigned to unit.74 (nhlk).

3.3.5.3. THMLAKE Output

Subroutine OUTLAKE writes the THMLAKE data to output file when the write-up time is due. It is described in "mo_outlake.f90", and called in the subroutine THMLAKE. This file is assigned to unit.75 (nglk). The file name is in the format of "exp_yymm.lk", where "exp" means experiment identity of the run, and yymm means the year and month of the simulation.

3.3.5.4. Diagnostic Output

Two files take down the diagnostic information. One is "lake.message", another one is "lake.diag". Subroutine LKERR records error message of thermocline simulation in "lake.message". This file is assigned to unit.77 (nlk1) and the LKERR function is controlled by the logical variable "Loperr" described in subroutine LAKEPHY. Subroutine OUTPUT records lake and lake grid information in "lake.message". This file is assigned to unit.78 (nlk2) and the OUTPUT function is controlled by the logical variable "Lopdia" described in subroutine LAKEPHY.

3.3.6. Logical Control Variables

Several logical variables are set in the THMLAKE to control the run.

Lbiglake	Set in subroutine LAKESST. Determine whether the lake grid is big lake or small lake.
Lopdia	Set in subroutine LAKEPHY. Control subroutine OUTPUT to record lake and lake grid information in "lake.message".
Loperr	Set in subroutine LAKEPHY. Control subroutine LKERR to record error message of thermocline simulation in "lake.message".
Lptime	Set in the shell script for running ECHAM-5. Control the frequency of

	the rerun file write-up
Lthmlake	Set in "mo_lake.f90". Determine whether turn on the THMLAKE or not.
Lwlvlcorr	Set in subroutine LAKESST. Determine an artificial water flux to prevent undesired water level.
Lwtime	Set in the shell script for running ECHAM-5. Control the frequency of the output file write-up

4. Result

4.1. ECHAM-4 (Lake Part)

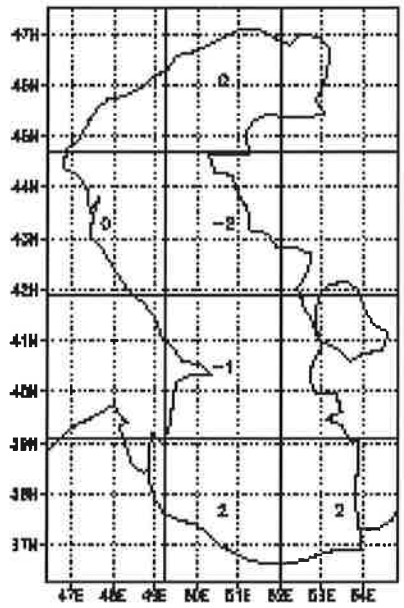

Figure 13 12-year mean (1981-1993) of net heat flux (positive upward) of ECHAM-4+THMLAKE run.

Figure 13 shows the simulated 12-year means (1982- 1993) of net heat flux by ECHAM-4+THMLAKE model over the Caspian Sea. Figure 14 shows the simulated 12-year means of composite monthly net heat flux. Figure 15 shows the simulated 12-year means of SST, current and ice. The sum of net heat fluxes of all the lake grids over the Caspian Sea was zero. This proves that the inclusion of the THMLAKE routine in ECHAM-4 make the energy budget closed over the Caspian Sea. In addition, the 12-year means

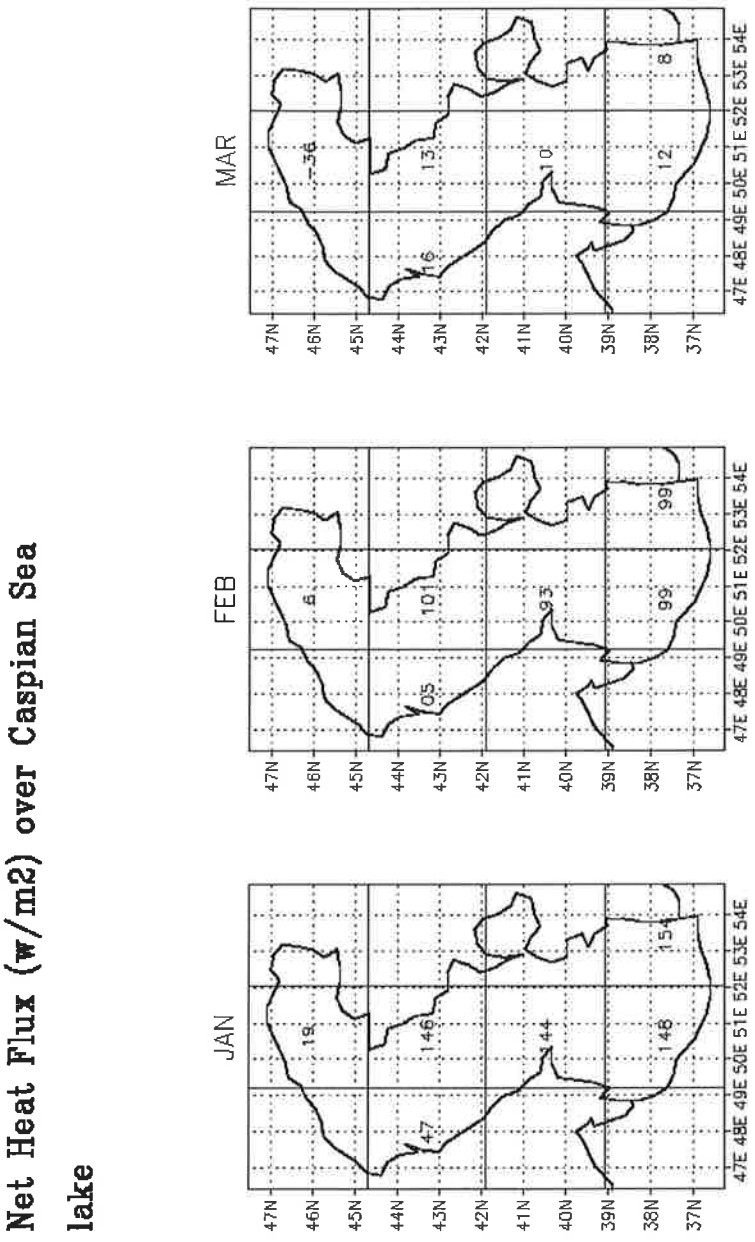

Figure 14 12-year mean (1981-1993) of composite monthly net heat flux (positive upward) of ECHAM-4+THMLAKE run.

Net Heat Flux (w/m2) over Caspian Sea lake

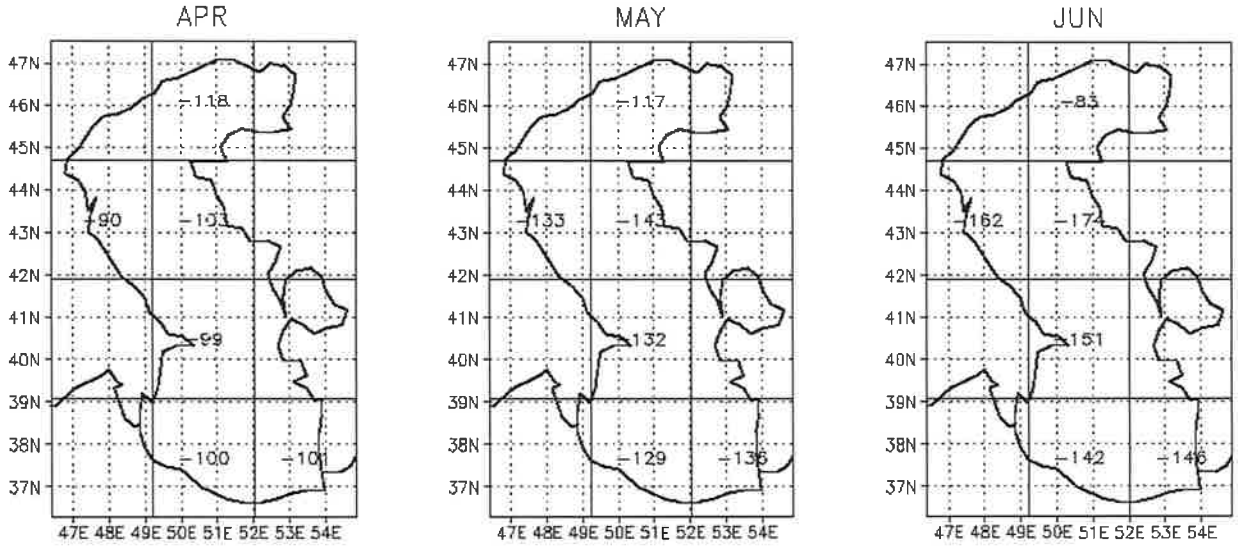

Net Heat Flux (w/m2) over Caspian Sea

lake

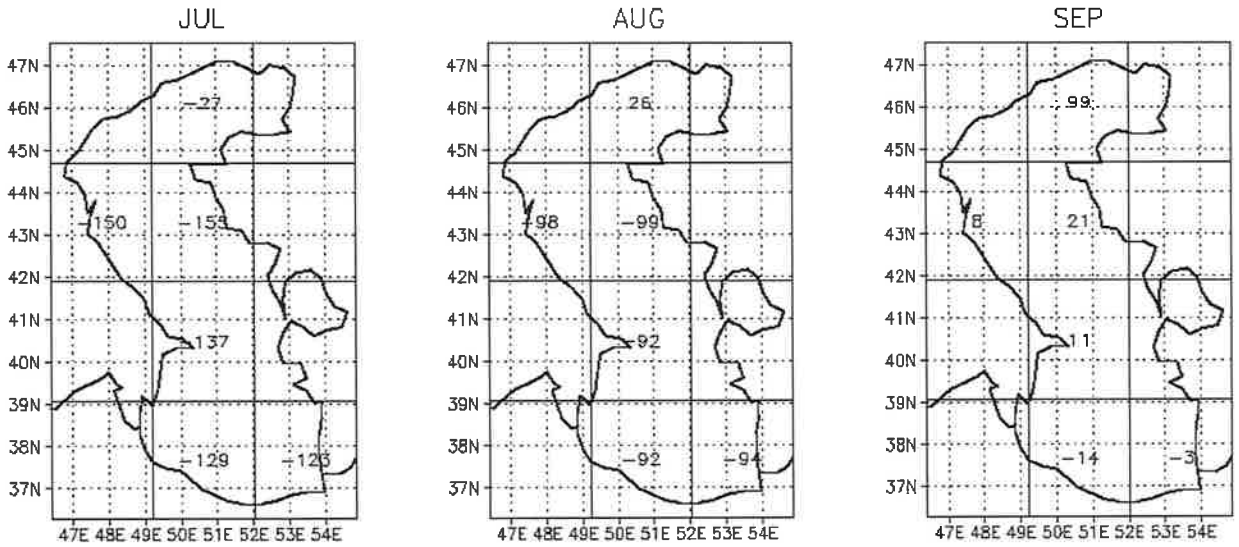

Net Heat Flux (w/m2) over Caspian Sea lake

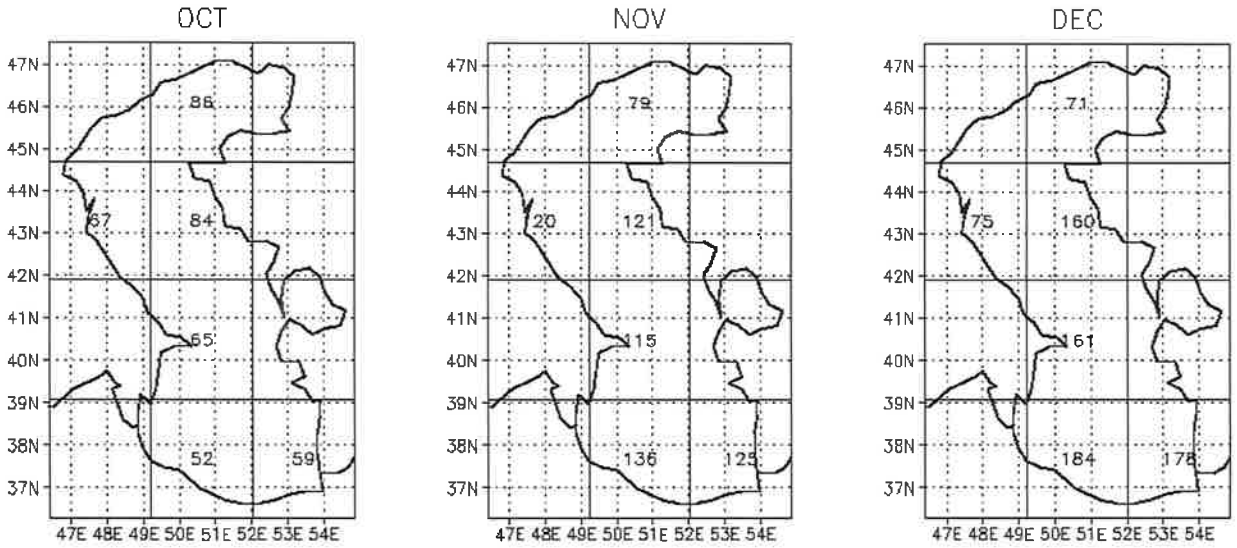

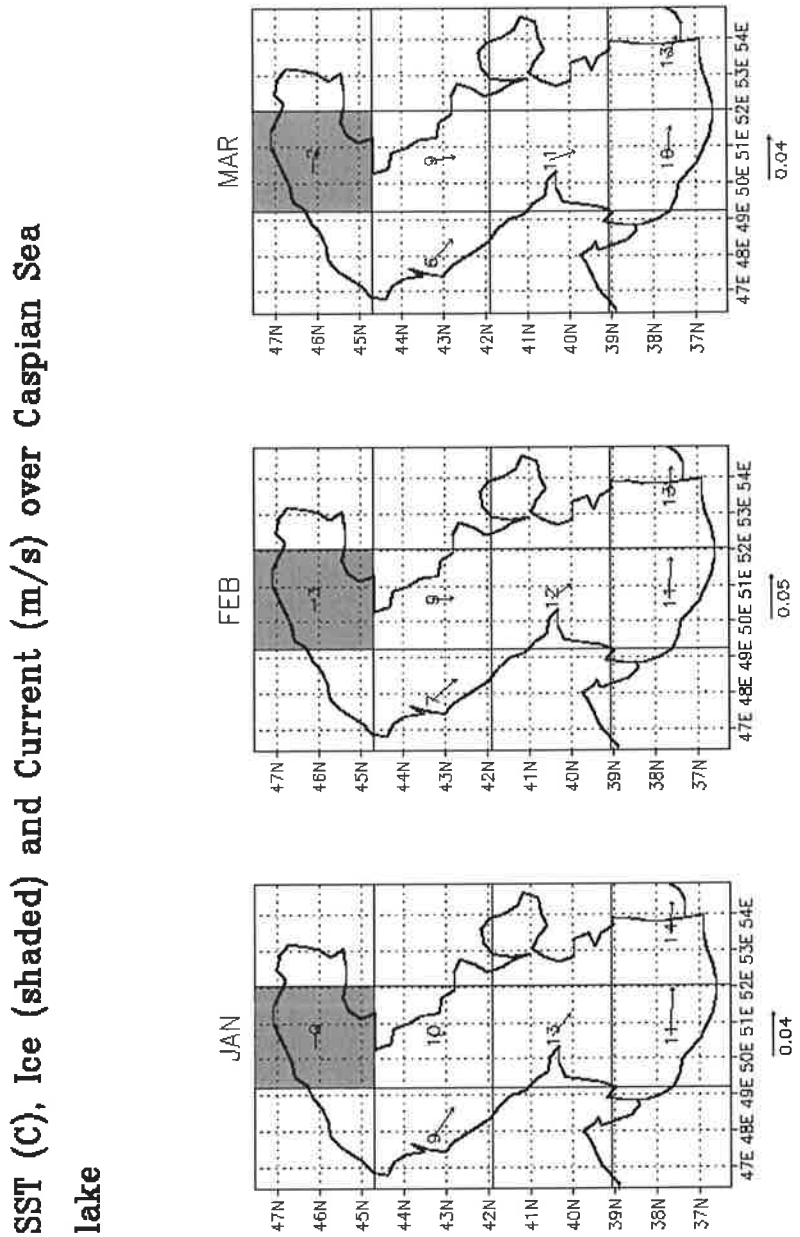

Figure 15 Simulated 12-year means (1982- 1993) of SST, current and ice by ECHAM-4+THMLAKE.

SST (C), Ice (shaded) and Current (m/s) over Caspian Sea lake

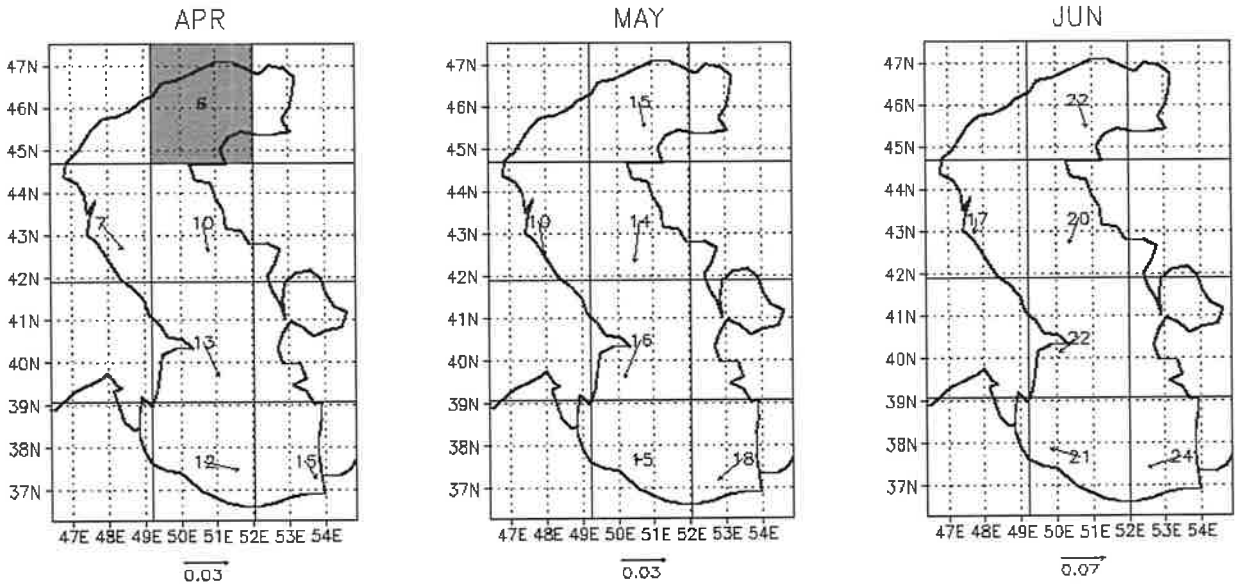

SST (C), Ice (shaded) and Current (m/s) over Caspian Sea lake

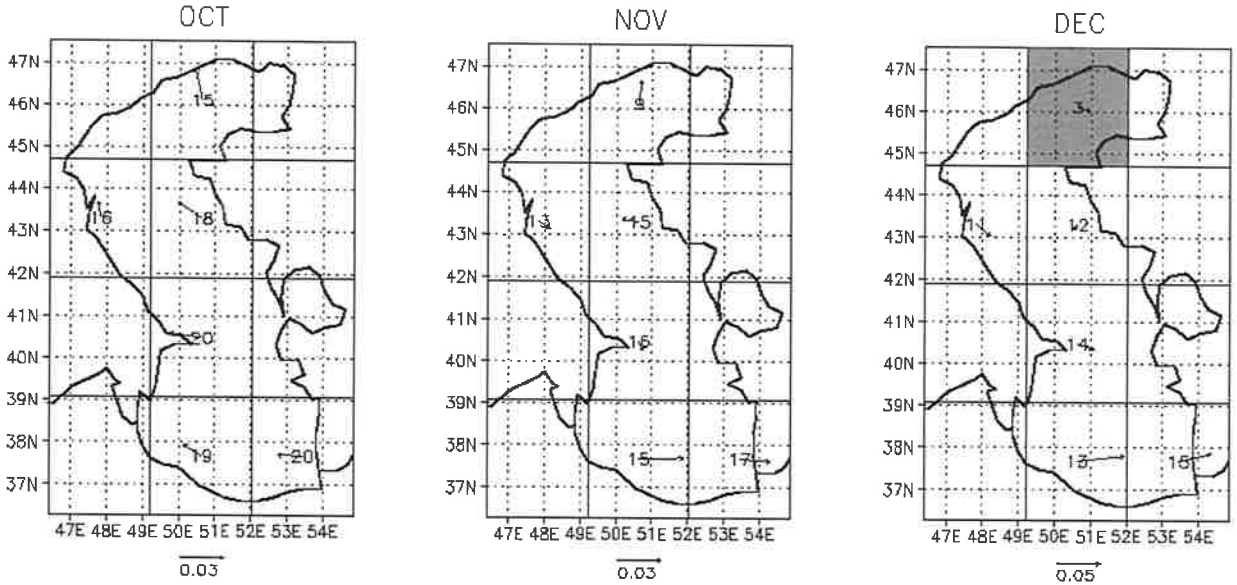

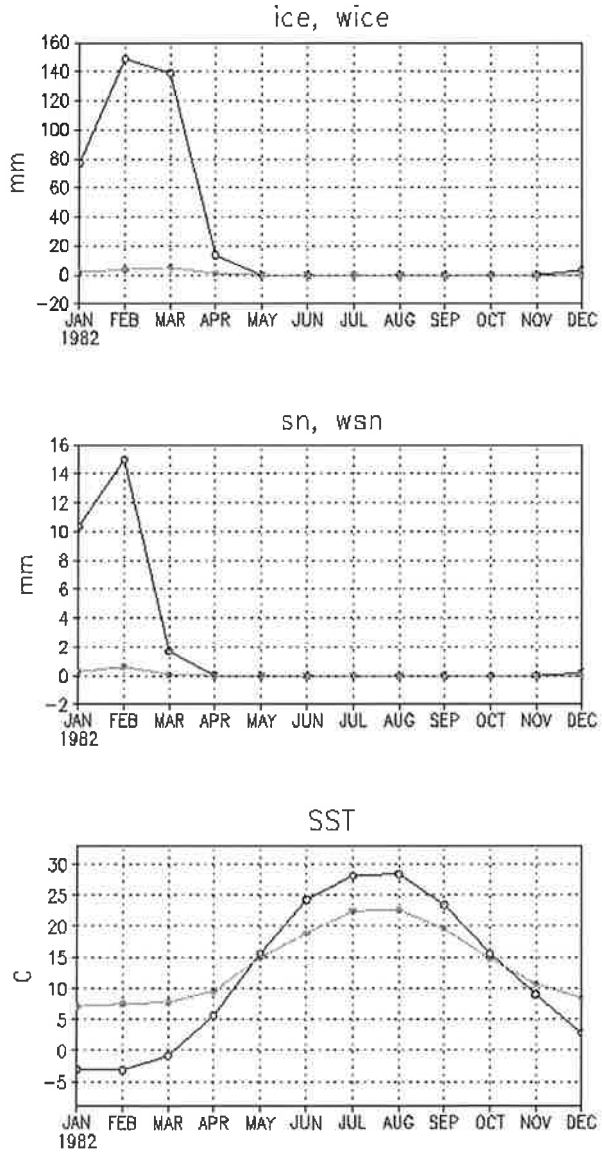

Figure 16 Simulated 12-year mean of ice thickness (ice), liquid water content in ice (wice), snow thickness (sn) and liquid water content in snow (wsn) at Caspian N (mm in liquid water), and a comparison between simulated SST and AMIP data set at Caspian N.

of net heat flux of each grid are in the range of –2 to 2 W m^{-2}, which are from the horizontal advection heat flux of each grid simulated by the aforementioned method. These values may be too small in comparison to the reality. Figure 14 shows that all the lake grids were gaining energy from April to August and losing energy from October to February except for the most northern grid (Caspian N). According to Figure 15, at Caspian N, the water was frozen during wintertime. This is the only grid having ice in the Caspian Sea and the ice period starts from December and lasts until April during the coldest year (Figure 16).

The simulated SST and ice period can be compared with observations (SA and VMGO, 1991; AMIP, Reynolds 1988). SA and VMGO (1991) shows that the most northern part of the Caspian was frozen starting from November and lasts until March (Figure 17). Figure 18 shows a comparison between SST simulated by the run and the AMIP data set. The difference of SST between the model output and the AMIP data set were within the range of –3 ~ +4 degree for all the grids except for the Caspian N grid. In winter at Caspian N, the SST of the AMIP data set are higher than 0℃, which is wrong. However, Figure 15 shows the simulated SSTs were not homogeneous distributed within the grids over the Caspian Sea. Horizontal advection-and-diffusion terms may be needed to remedy the error. Especially the 28℃ at the Caspian Sea N in August seems too high.

According to SA and VMGO, the current in the southern part of the Caspian Sea is clockwise from March to August and counter-clockwise from September to February (except for November). In the model, the current was driven by the wind shear only. The model did not modify the current due to thermal expansion, water level difference and the friction at the horizontal boundaries. Nonetheless, the simulated current shows that it is clockwise from May to October and counter-clockwise from November to April.

There is a time lag of one month for water at Caspian N to freeze in the model. Possible reasons of the time lag include 1) the albedo parameterization, 2) the skin layer parameterization, 3) the lack of horizontal advection-and-diffusion terms in the model, and 4) an error due to ECHAM-4. Figure 16 shows a 12-year means of monthly thickness of ice and snow, and a comparison of SST simulated by the model and from the AMIP data set. It shows that the maximum thickness of ice occurred in February with a value of 149 mm. It also shows that there was snow over ice from December to March. During the snow period, the albedo should be higher than with ice only. Figure 19 shows the simulated albedo in February 1992. The albedo at the most northern grid is much higher than the other Caspian grids since water was frozen there.

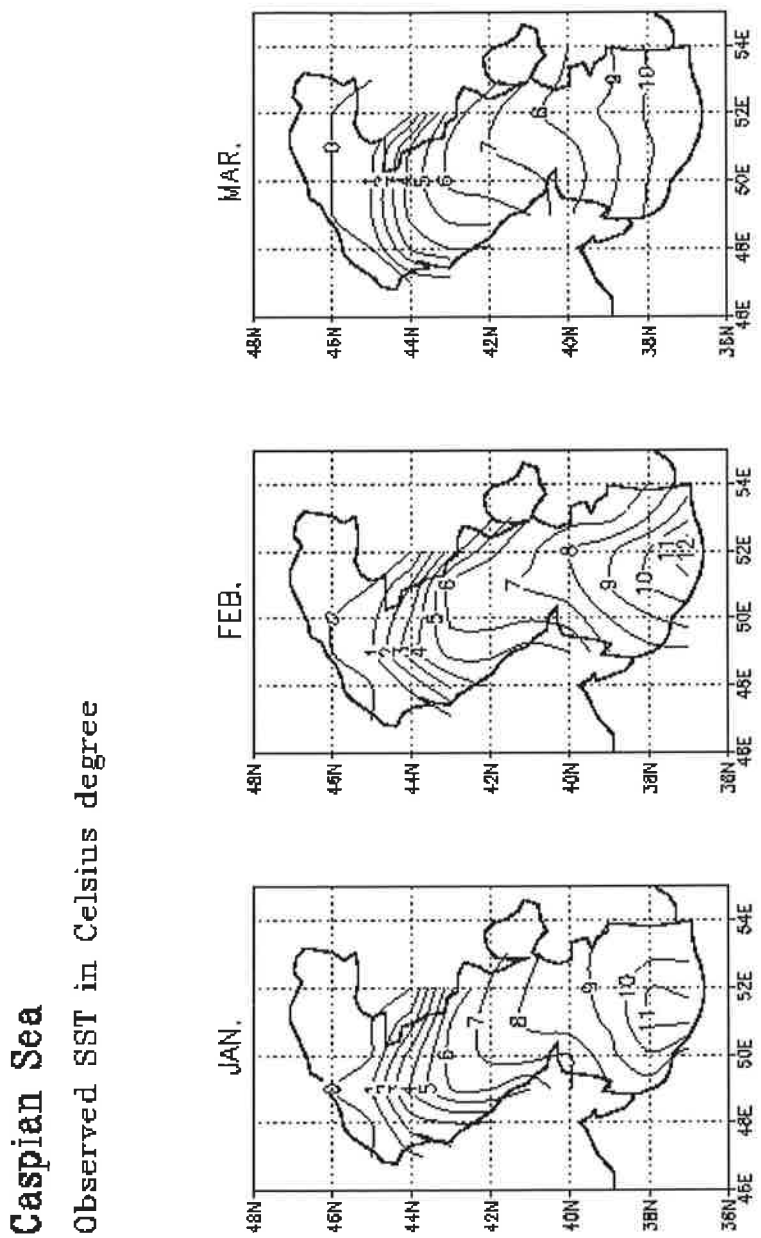

Figure 17 Digitized observed SST over the Caspian Sea.

Caspian Sea

Observed SST in Celsius degree

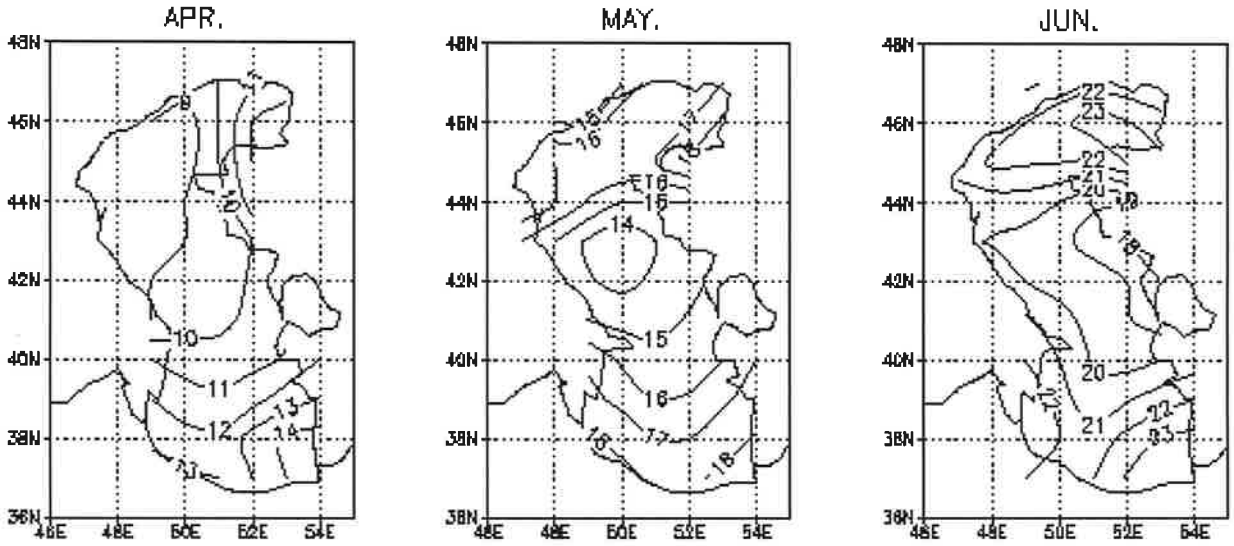

Caspian Sea

Observed SST in Celsius degree

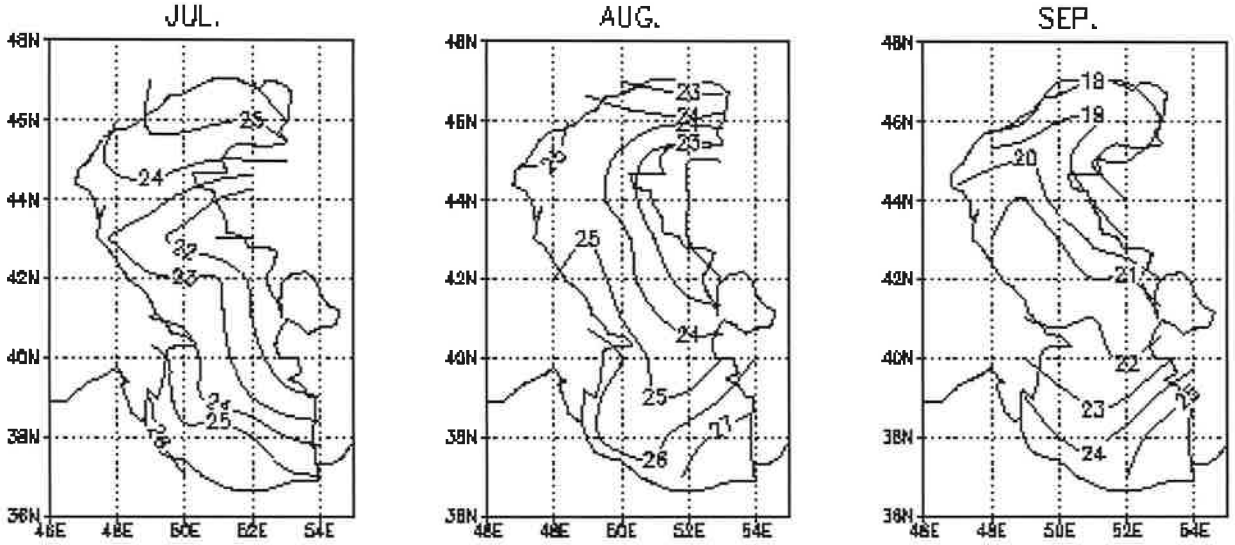

Caspian Sea

Observed SST in Celsius degree

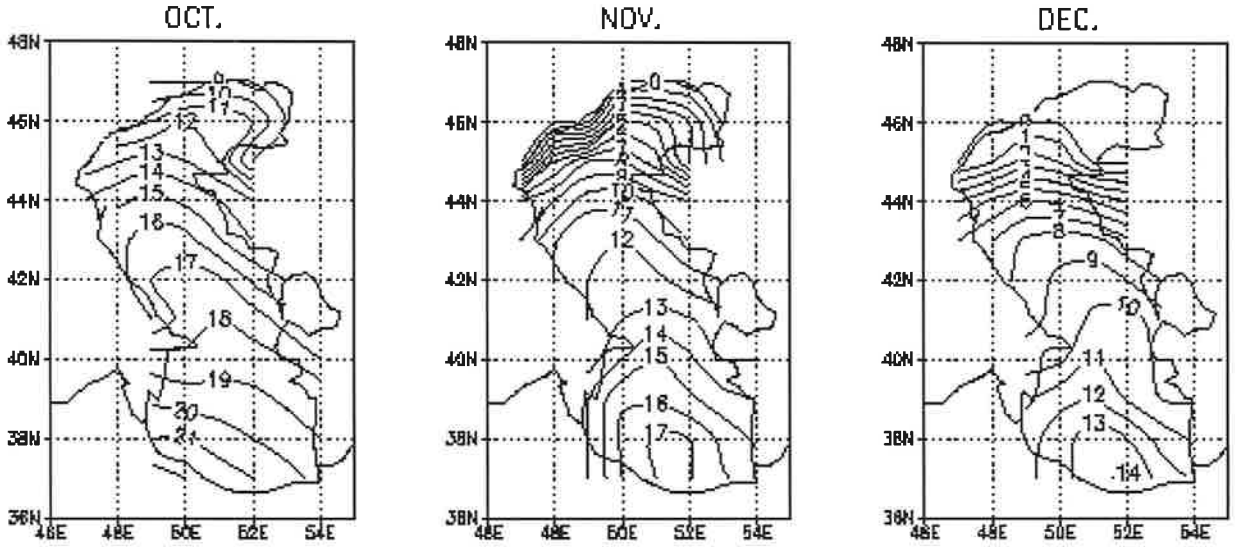

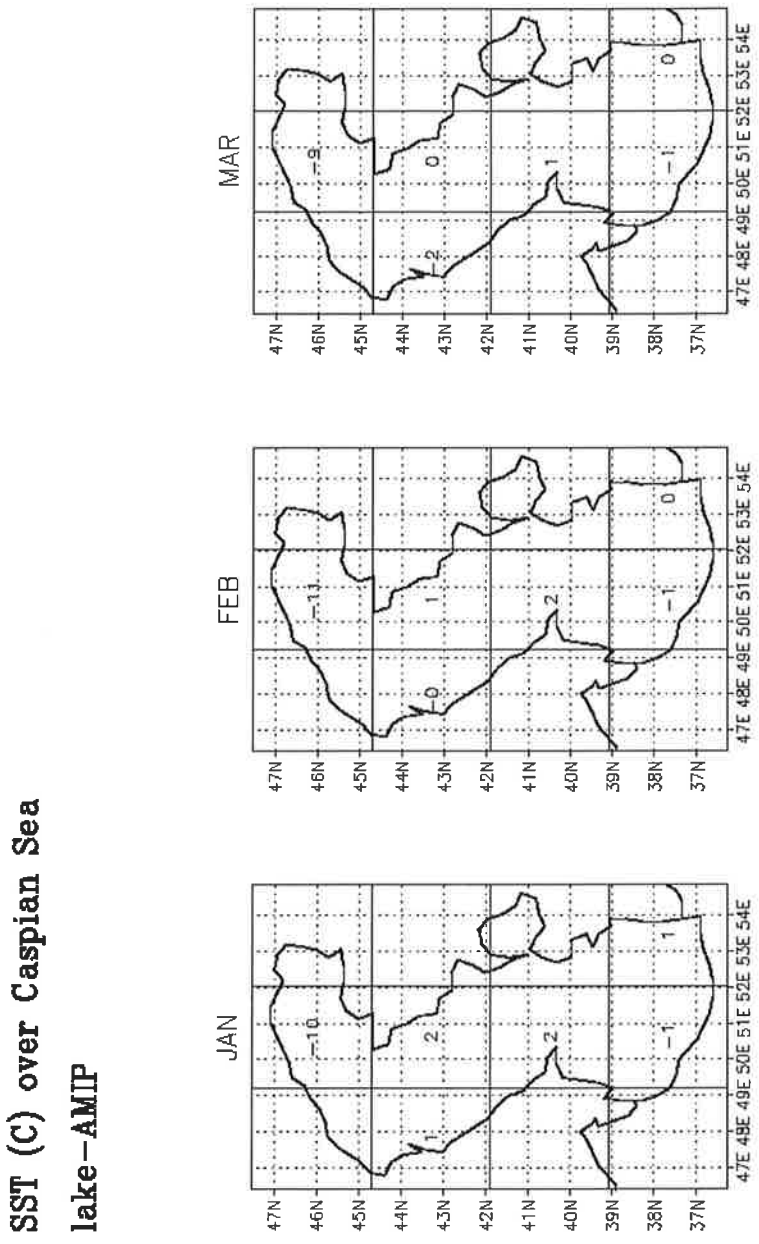

Figure 18 Difference of monthly SST over the Caspian Sea between ECHAM-4+THMLAKE and AMIP data set.

SST (C) over Caspian Sea

lake-AMIP

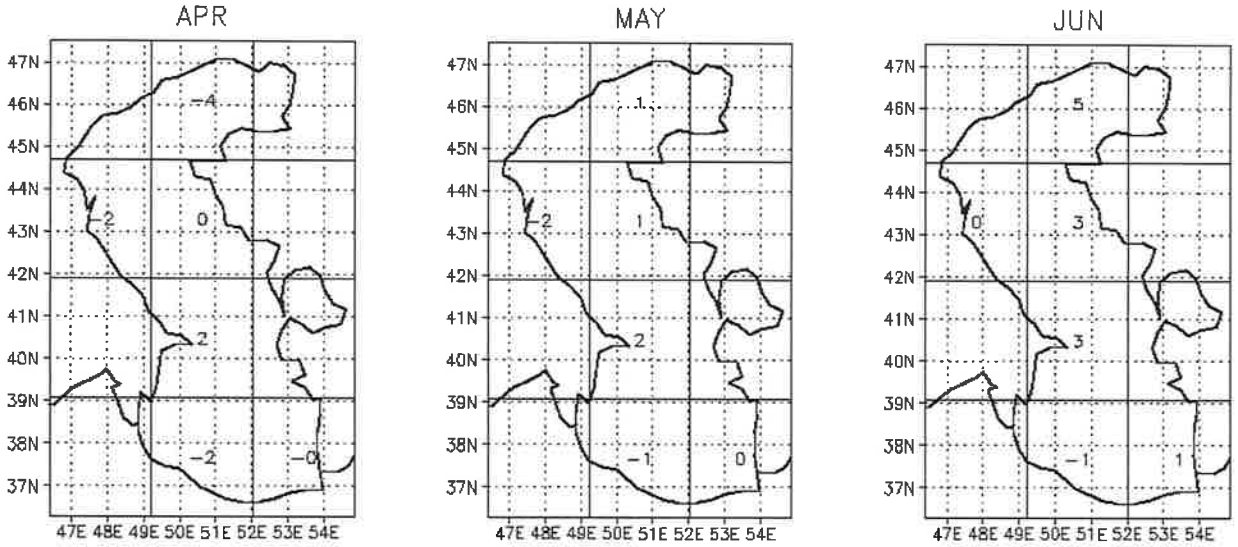

SST (C) over Caspian Sea

lake−AMIP

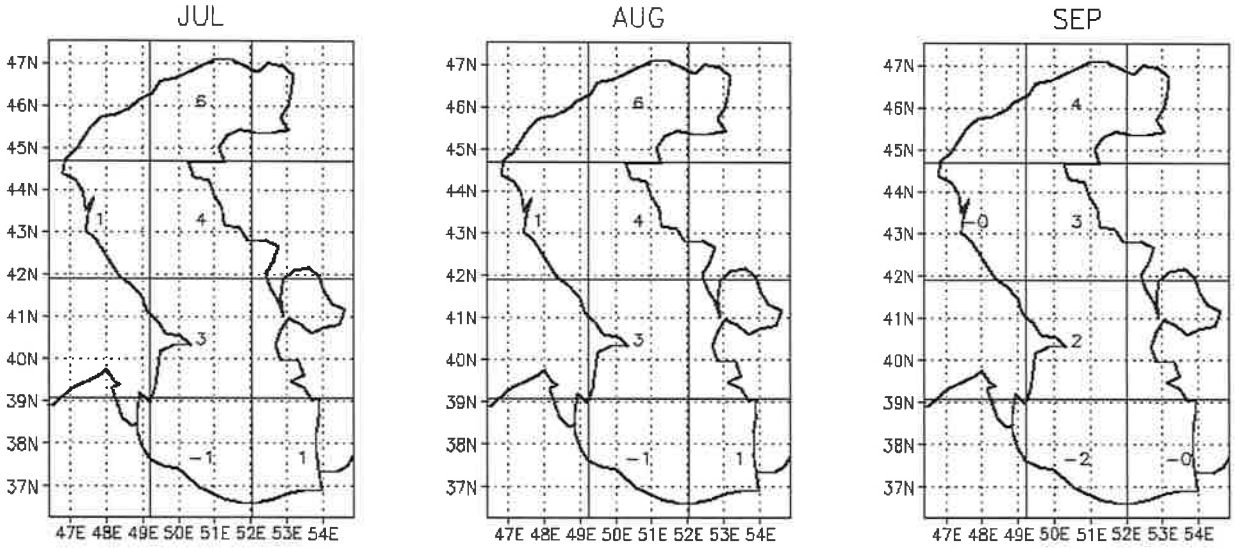

SST (C) over Caspian Sea

lake−AMIP

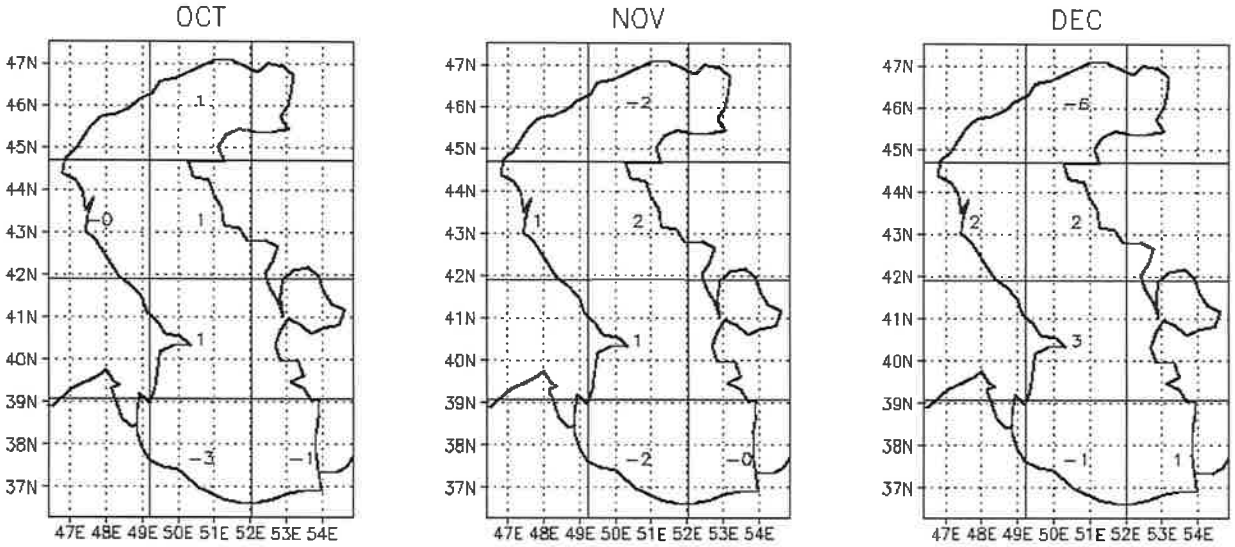

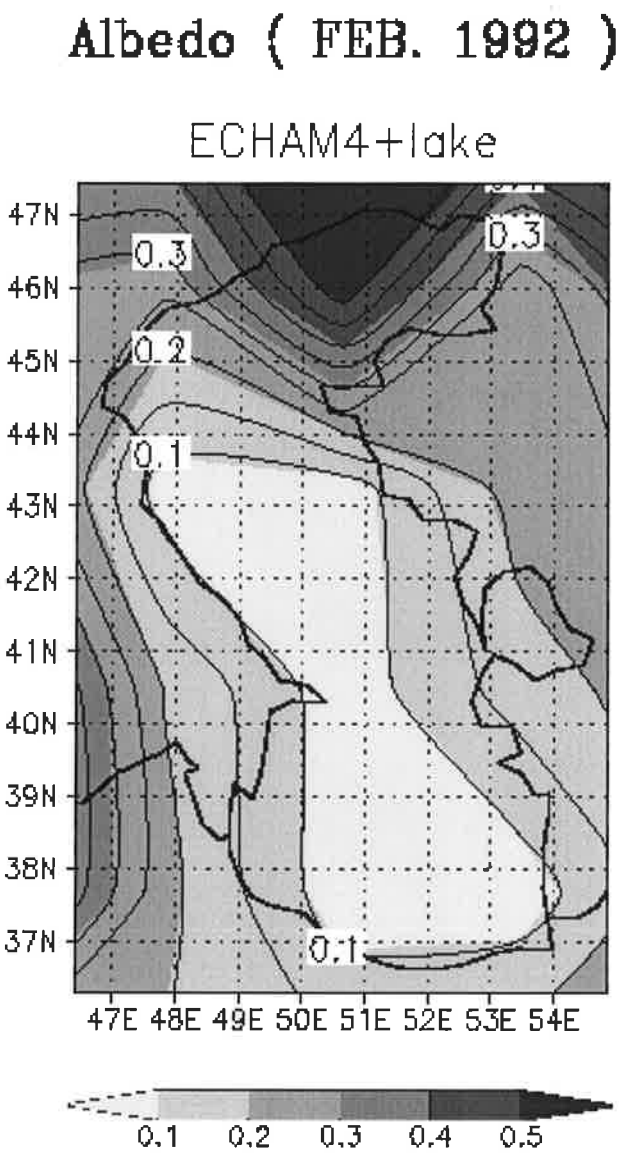

Figure 19 Albedo simulated by ECHAM-4+THMLAKE in February 1992.

According to the simulated 12-year monthly means (1982 ~ 1993) of inter-basin outflow (mm per month) by the ECHAM-4+THMLAKE model over the Caspian Sea (not shown here), water outflows from the most northern grid of the Caspian Sea to the other grids from March to October. It is because water evaporates during warm months and get supply at the most northern grid from the Volga River. The maximum outflow of the most northern grid is in May. During wintertime from November to February, water flows into middle northwest and middle north grids. The supplies are not only from the most northern grid but also the southern grid.

According to the simulated 12-years monthly means (1982 ~ 1993) of river inflow with water-level-corrected (mm per month) by the ECHAM-4+THMLAKE model over the Caspian Sea (not shown here), the value of each grid implies the external inflow or outflow of water. Excluding the most northern grid, the water level is lowered by the correction by 138 to 147 mm per month. The monthly differences of the most northern grid suggest the discharge variation of the Volga River. The maximum inflow is in May, and with low inflow from December to February. The outflow of the most northern grid increases with the discharge of the Volga River and reaches the maximum in May. The minimum outflow is in winter when the river discharge is low.

According to the simulated 12-year monthly means (1982 ~ 1993) of salinity (PSU) by ECHAM-4+THMLAKE model over the Caspian Sea (not shown here), excluding the northern grid, where the Volga River flows into, the salinity of the other grids are between 11.8 and 12.1 and with tiny monthly differences. Comparing simulations to observed salinity (Kosarev and Yablonskaya, 1994) shows satisfactory results. In the northern part of the Caspian Sea, the simulation is about 0.5 PSU lower than observation. In the southern part, it is higher for about 1.0 PSU.

Figure 20 shows the simulated monthly average (1991 Apr.- 1993 Apr.) of water temperature, salinity, current, heat diffusivity, TKE and mixing length at the Caspian Sea by ECHAM-4+THMLAKE. In the most northern grid (N), there is no vertical discrepancy of temperature and salinity as the water is shallow. Highest temperature occurs on August, and lowest temperatures, which are under freezing point, occur on February. Maximum salinity is in March, i.e. before the melting. The fresh water from Volga River reaches the maximum on May and starts diluting salinity. Also, ice is fresh water and the melting dilutes seawater. When the inflow from Volga River decreases in winter and some fresh water freezes, salinity increases. In the middle northwest grid, the water depth is about 70 meters. The maximum temperature at the surface occurs in August and energy is transported into deeper water, where the maximum temperature occurs 2~3 month later than at the surface. Salinity varies only near the surface during spring and summer, and keeps constant value in deeper water. The current driven by wind shows the wind direction of northwest during winter and spring in this grid. Annual cycles of heat diffusivity, TKE and mixing length are the same, and the trends match the surface current which is strongly related to the wind.

In the middle north grid of the Caspian Sea, water temperature underneath 60 meters is nearly constant. The pattern of salinity is similar to the water temperature. The current in this grid differs from the mNW grid. In summer time, the current driven by wind is to the northeast; in winter, the direction is the same as in the middle northwest grid. Trends of heat diffusivity, TKE and mixing length are highly

interrelated. Values of the above three properties increase during winter when the current (wind) is strong and decrease in the rest time when the current is weak. In the middle south and the south grids, all the properties, except salinity, are similar to the middle north grid. Because the depths of these two grids are deeper than other grids, salinity in deeper water remains constant and is higher than in shallow water. Salinity in shallow water is strongly effected by inflow and outflow of the grid. The situation in the southeast grid differs from the middle south and south grid. Water of this grid is shallower than the previous two grids, there is hardly any stratification in the salinity and temperature in deep water is strongly effected by energy transported from surface.

According to the profiles of water temperature, salinity, current, heat diffusivity, turbulent kinetic energy, mixing length from 1982 ~ 1993 (not shown here), the thermal stratification is not apparent in February, but is well developed in August. The thermal structure will cause turnover. During the turnover period, heat diffusivity, TKE and mixing length are larger than the stratification period. Water in the most northern grid is shallow. It makes the temperature cooler than other grids in February and warmer in August. Salinity is stable and there are only small differences between February and August.

Figure 21 shows the simulated monthly means of snow depth, ice depth, liquid water in snow, liquid water in ice, SST and AMIP SST in the most northern grid of the Caspian Sea from October 1981 to September 1984. The simulation in this grid shows that the water was frozen, but in AMIP it is not. The figure shows that the depth of snow fluctuates severely from 0.4 to 70 mm, and the depth of ice varies from 20 to 300 mm. The simulated SST is higher than AMIP in summer time, and cooler than AMIP in wintertime. The amplitude of simulated SST is in the range of -7 ~ 30 ℃, but for AMIP the SST is only 5~25℃. Table 1 shows the simulated frequency of snow and ice. In January and February, it freezes in each of the 12 years simulation. The iced period for the simulation is from December to April, there is about 1-month delay compared to the observation of SA and VMGO (1991).

Table 1 Simulated snow and ice frequency of ECHAM-4+THMLAKE at the Caspian Sea N, 46.1105N, 50.625E in 12 years from Oct. 1981 to Dec. 1993

month	December	January	February	March	April
Frequency of Snow	2	12	12	8	0
Frequency of Ice	2	12	12	10	4

Figure 21 shows monthly means of simulated SSTs and AMIP SSTs in the Caspian Sea from October 1981 to September 1984. There is a large difference

between simulation and AMIP SST in the most northern grid. Nevertheless, the simulation may be closer to reality than AMIP. In the middle northwest grid, the simulation lags behind AMIP by about 2 months during wintertime. In the middle north grid, time lag problem still exits. The simulation overestimates the temperature by about 5℃ in summertime. In the middle south grid, the simulation is similar to in the middle north grid. ECHAM-4+THMLAKE always underestimates SST slightly in the most southern grid. As for the southeast grid, simulation is closest to the AMIP SST in the Caspian Sea. In summarizing, simulations and AMIP are acceptable similar except in the most northern grid. Some grids overestimate SST, and some underestimate. The problem can be improved by considering diffusion and advection term to distribute energy imbalances in different grids.

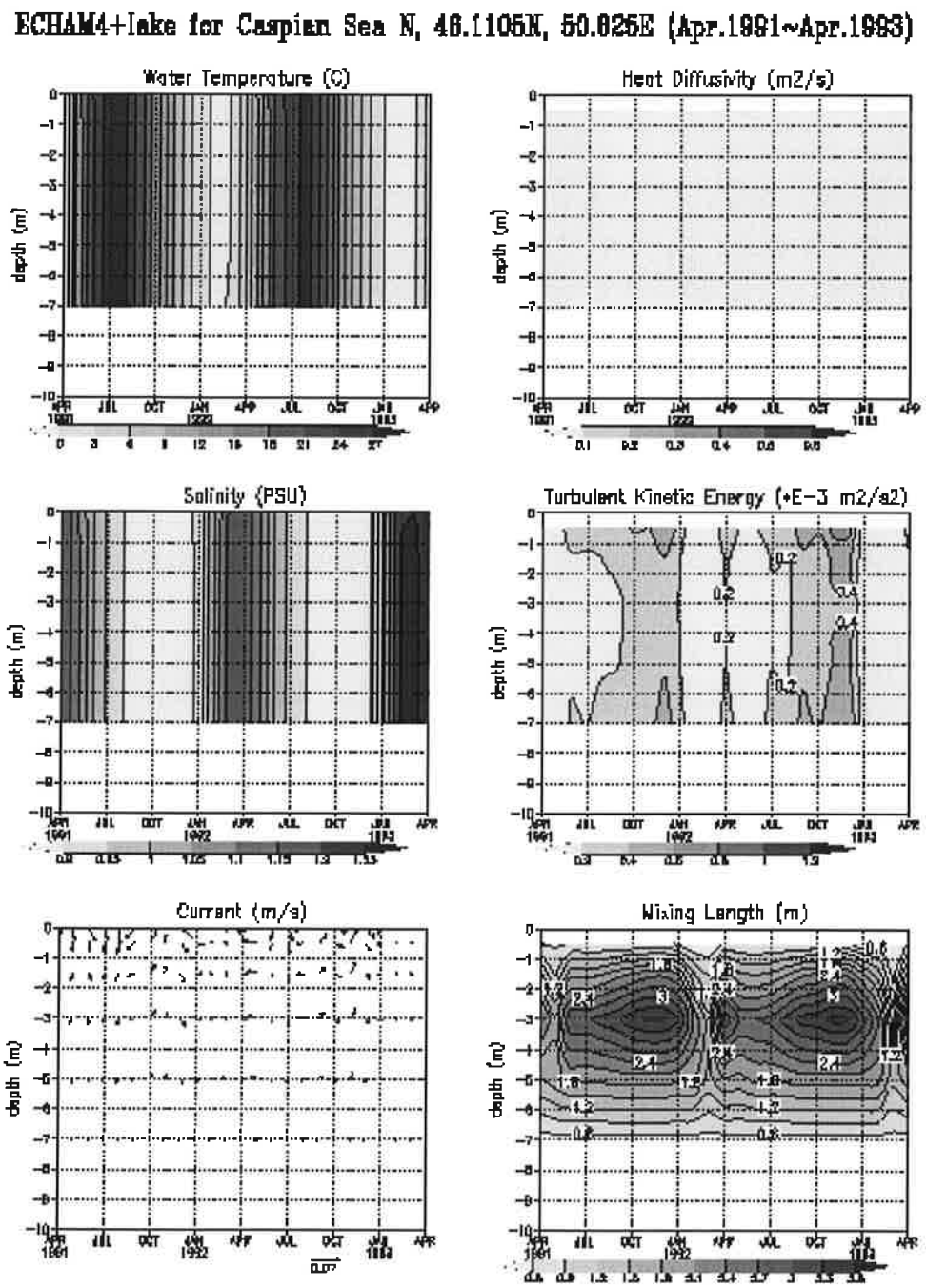

Figure 20 Simulated monthly averages(1991 Apr.- 1993 Apr.) of water temperature, salinity, current, heat diffusivity, TKE and mixing length at the Caspian Sea by ECHAM-4+THMLAKE.

ECHAM4+lake for Caspian Sea mNW, 43.298N, 47.8125E (Apr.1991~Apr.1993)

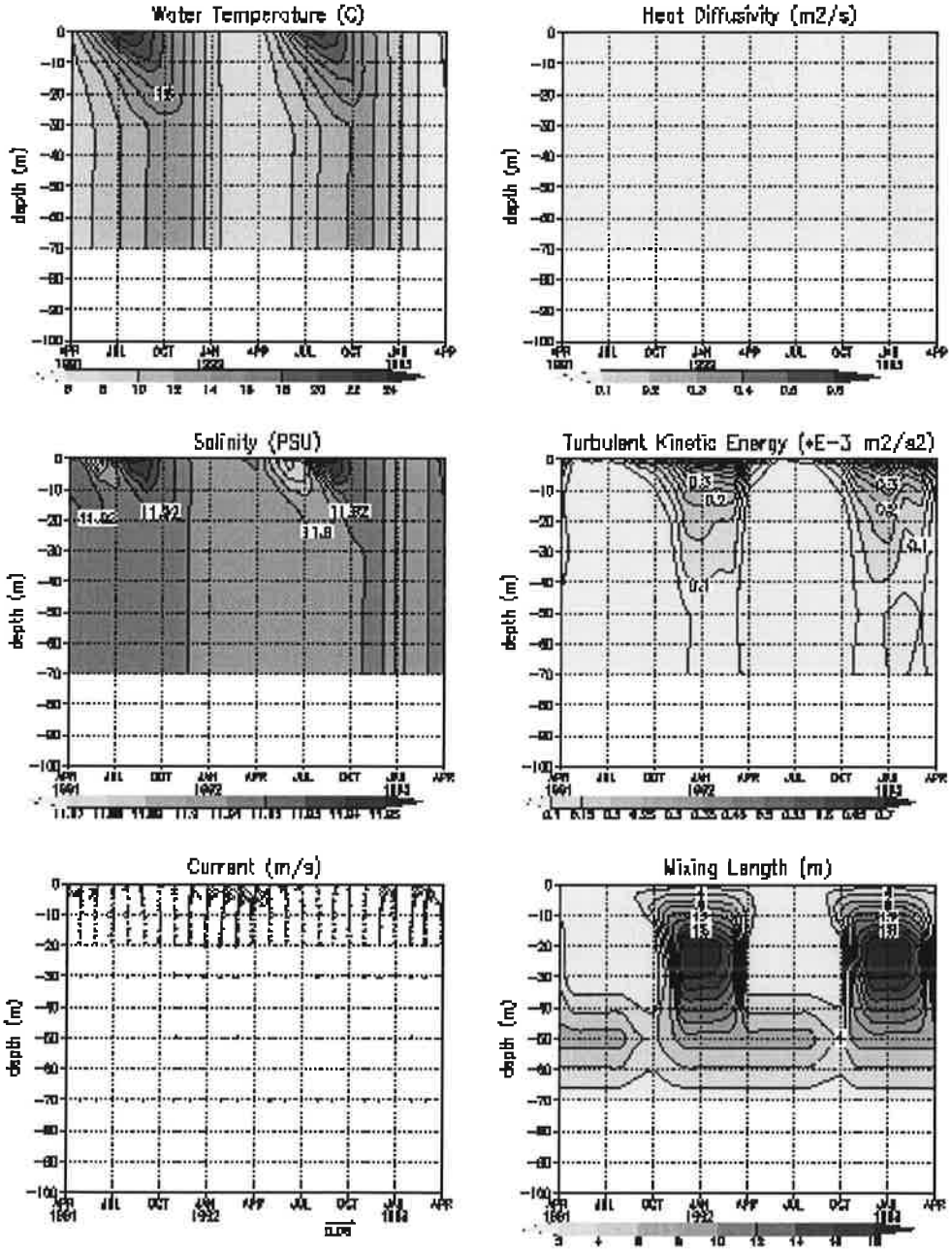

ECHAM4+lake for Caspian Sea mN, 43.295N, 50.625E (Apr.1991~Apr.1993)

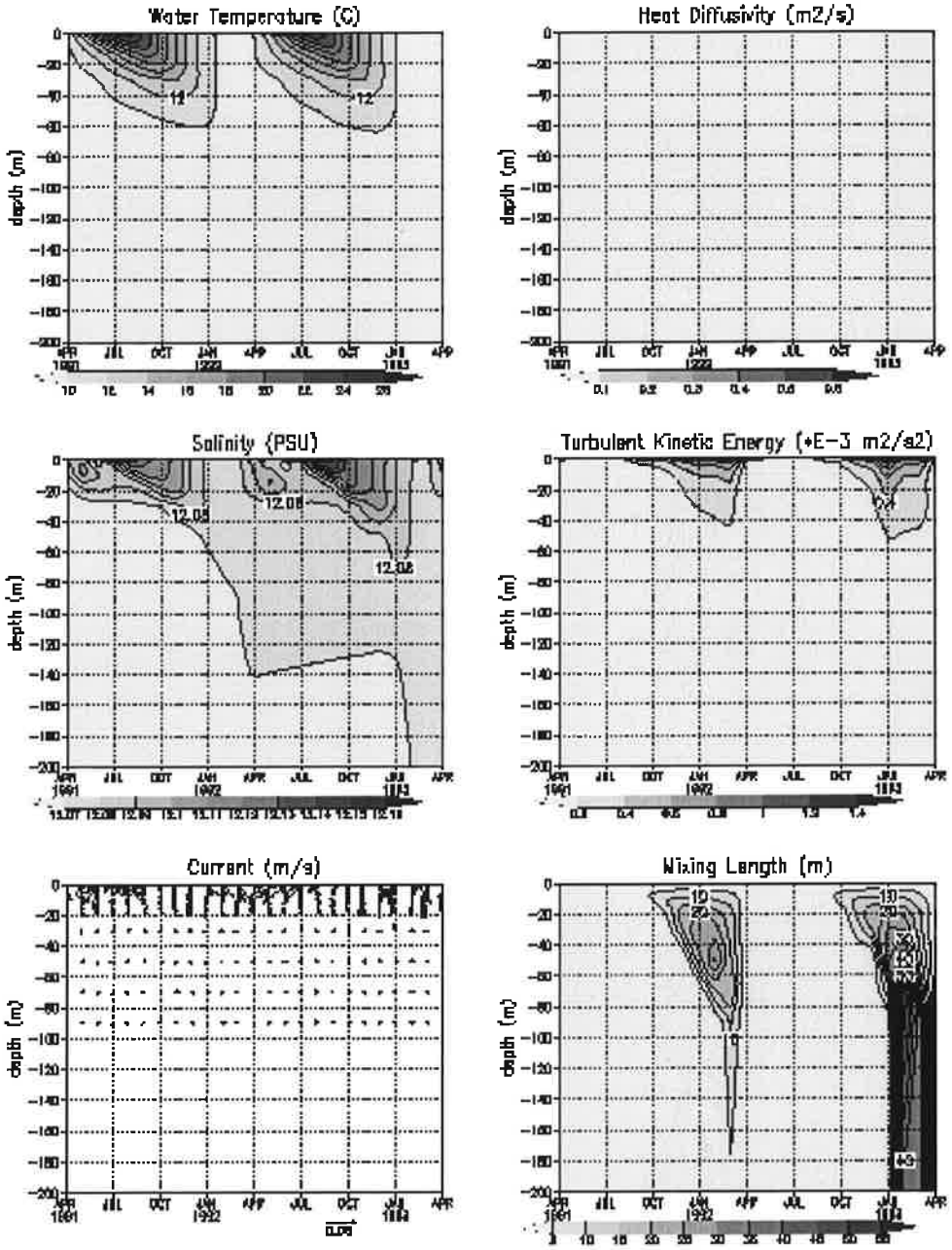

ECHAM4+lake for Caspian Sea mS, 40.4656N, 50.625E (Apr.1991~Apr.1993)

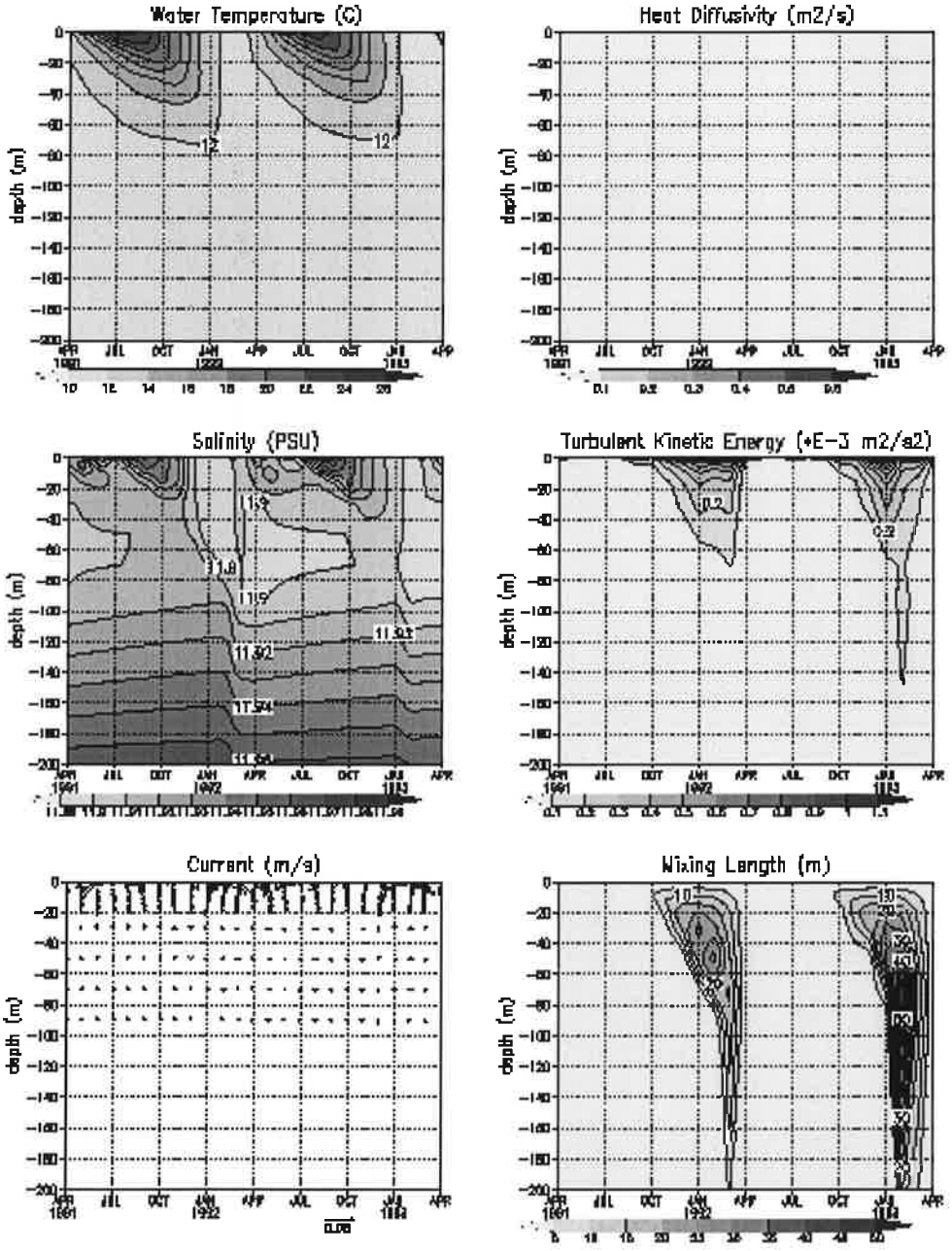

ECHAM4+lake for Caspian Sea S, 37.673N, 50.625E (Apr.1991~Apr.1993)

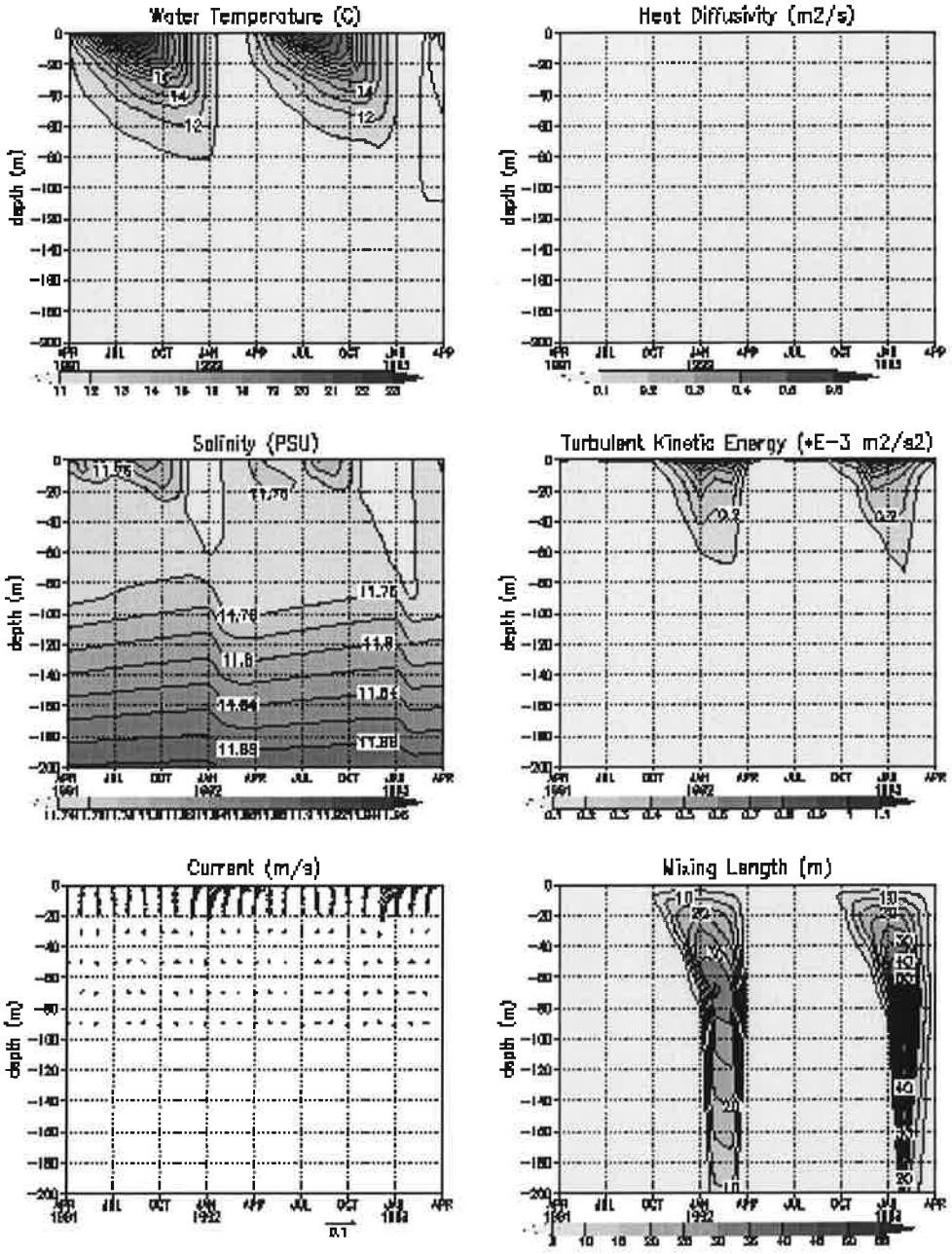

ECHAM4+lake for Caspian Sea SE, 37.673N, 53.4375E (Apr.1991~Apr.1993)

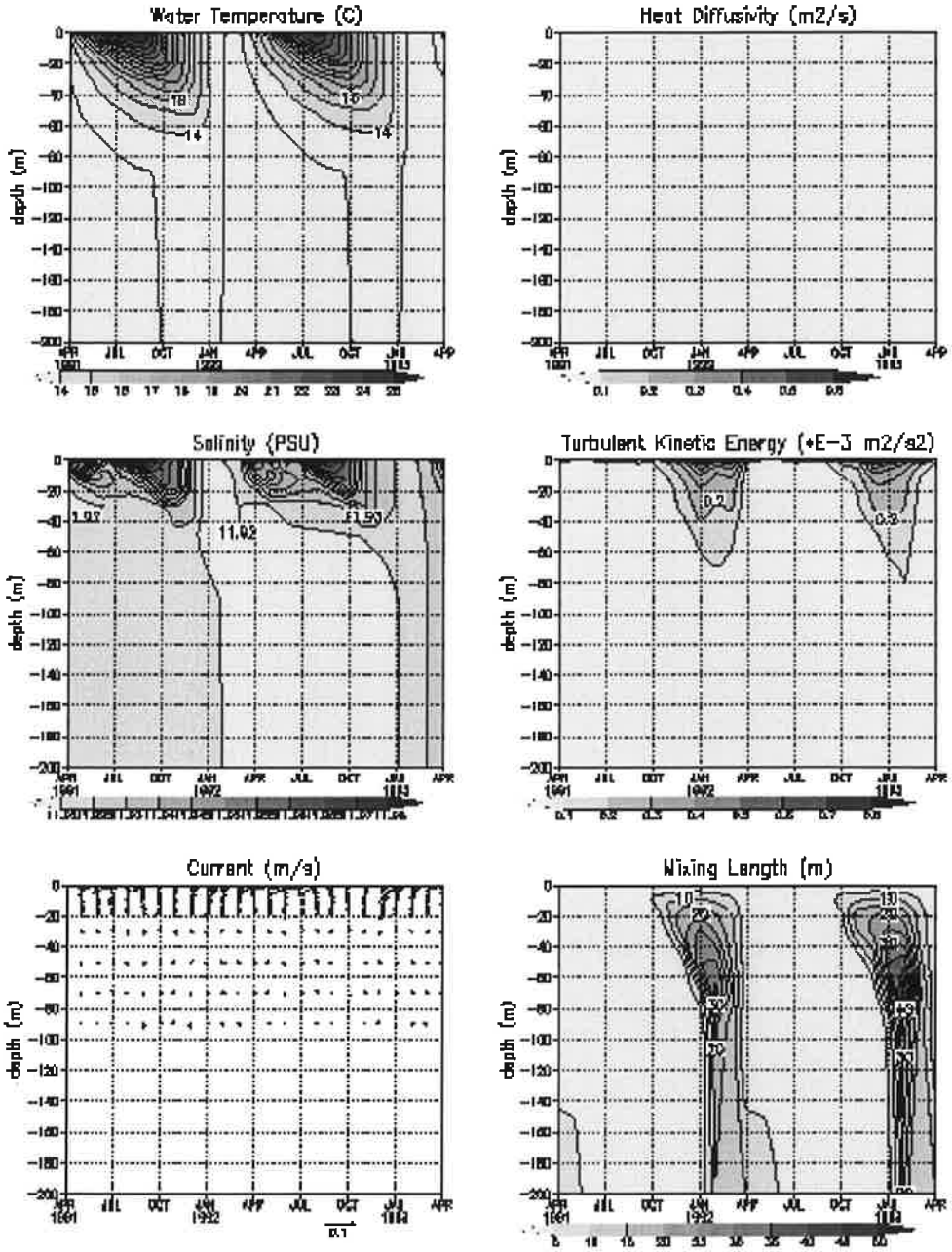

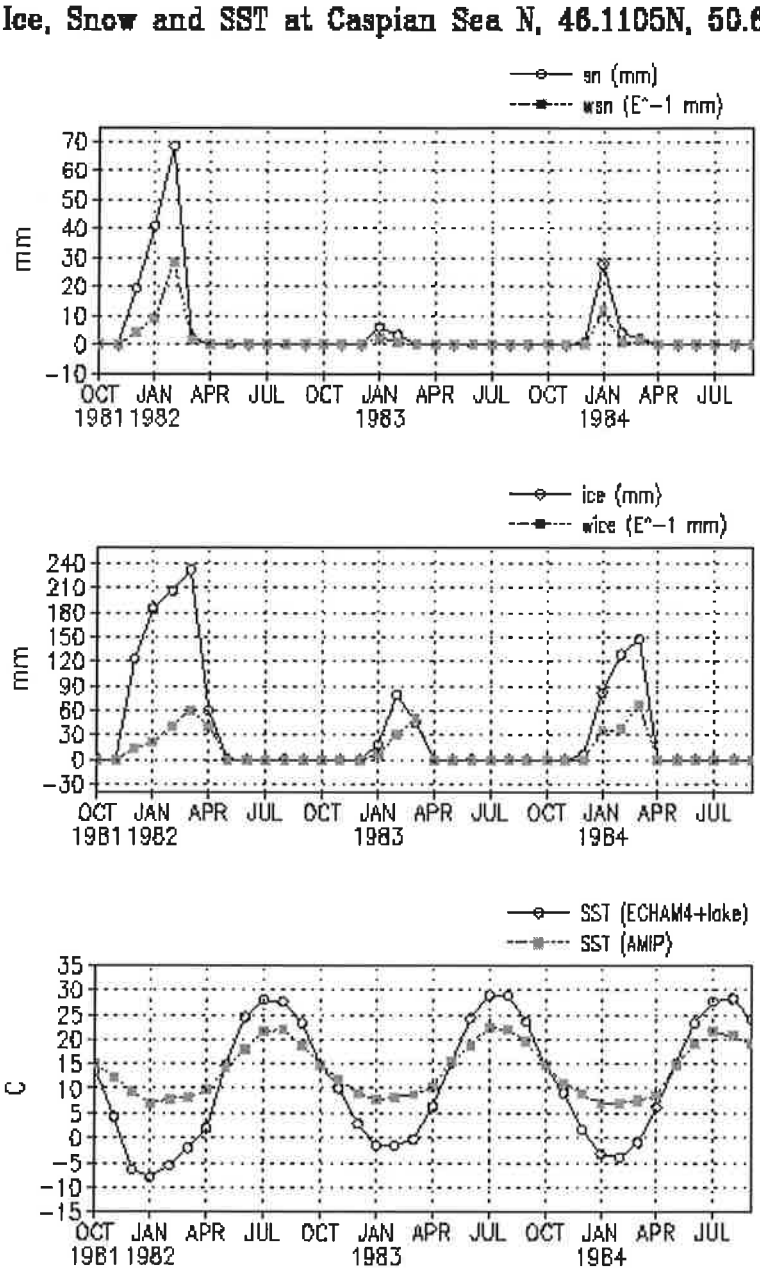

Figure 21 Simulated monthly means of dry snow depth, ice depth, liquid water in snow, liquid water in ice, SST and AMIP SST in the Caspian Sea N, 46.1105N, 50.625E, from October 1981 to September 1984.

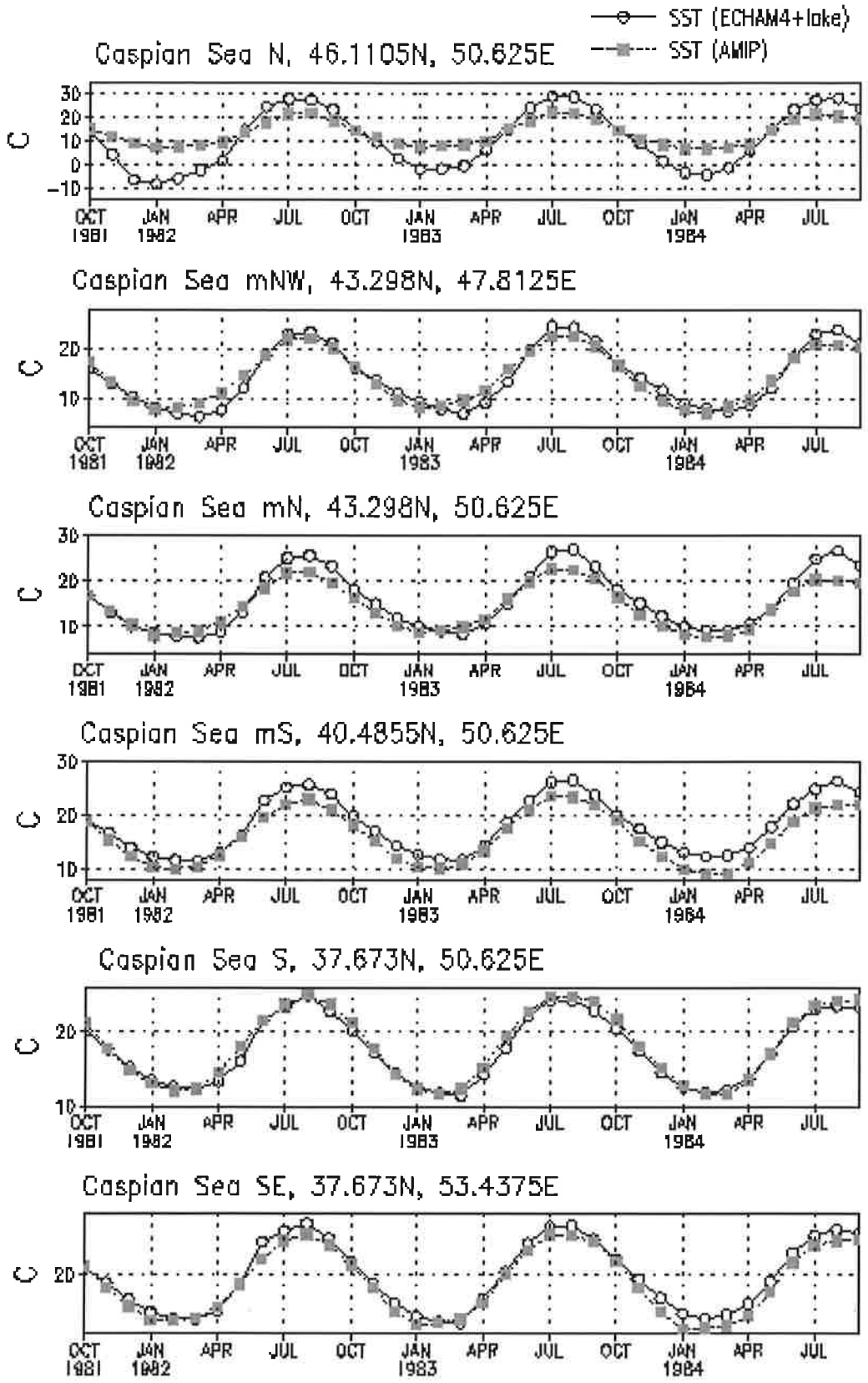

Figure 22 Monthly means of simulated SST and AMIP SST in the Caspian Sea from October 1981 to September 1984.

4.2. ECHAM-4 (Atmosphere Part)

For investigating the impact of the Caspian Sea on the atmosphere we have available several 10 year simulations with the ECHAM-4 model. One in which the SSTs of the Caspian Sea are prescribed by values provided by AMIP (AMIP), one in which the Caspian Sea was treated as land points (noCS) and one in which the SSTs in the Caspian Sea are calculated inter actively with THMLAKE routine (LAKE). All of them use the same prescribed ocean temperatures provided by AMIP. Our expectation is that the noCS run will have in winter much lower temperatures than the others and in summer much higher temperatures. The northern points of the Caspian Sea are very shallow and in the LAKE run one finds there ice cover in agreement with observations while the AMIP SSTs have values above zero. In this respect the LAKE run should be intermediate between the other two. This expectation is in agreement with the finding in Figure 23, where the surface temperature differences of the different runs are shown for the four seasons. The differences between the LAKE and the AMIP run are concentrated on the northern part of the Caspian Sea where the water is shallow while the differences between the noCS and LAKE run cover the whole Caspian Sea and surrounding areas. Larger differences not directly connected with the Caspian Sea can be found over Turkey which are connected with a large scale circulation (see below). Annual cycles of SSTs at the selected Caspian Sea grid points are shown in Figure 24. In extreme cases the temperatures deviate by more than 10K. The AMIP and LAKE SSTs differ most in the northern shallow area (Caspian N) where the AMIP SSTs do not reach the freezing level in winter and moderately warm temperatures in summer.

Direct impacts of such large SST differences can be expected in the latent heat flux over the sea (LHFX). There will be more evaporation over the sea when the water is warmer. However, in the case of the noCS run this simple relation is made more complicated because of the availability of water is not unlimited as in the two other cases. Figure 25 shows the LHFX differences. Generally one can see a straight correspondence - higher SSTs lead to higher LHFX - the main exception is JJA for the noCS - LAKE comparison when the LAKE run provides much more evaporation. Over the Caspian Sea in the noCS case there is hardly any water left in the soil leading to near zero evaporation while it is very large in both other cases with the Caspian Sea. A lack of evaporation over the Caspian Sea would lead to reduced atmospheric moisture over the Caspian Sea and its surrounding which would eventually lead to enhanced evaporation somewhere else and in our experiments we find this enhancement especially over the Black Sea where the prescribed SSTs are identical.

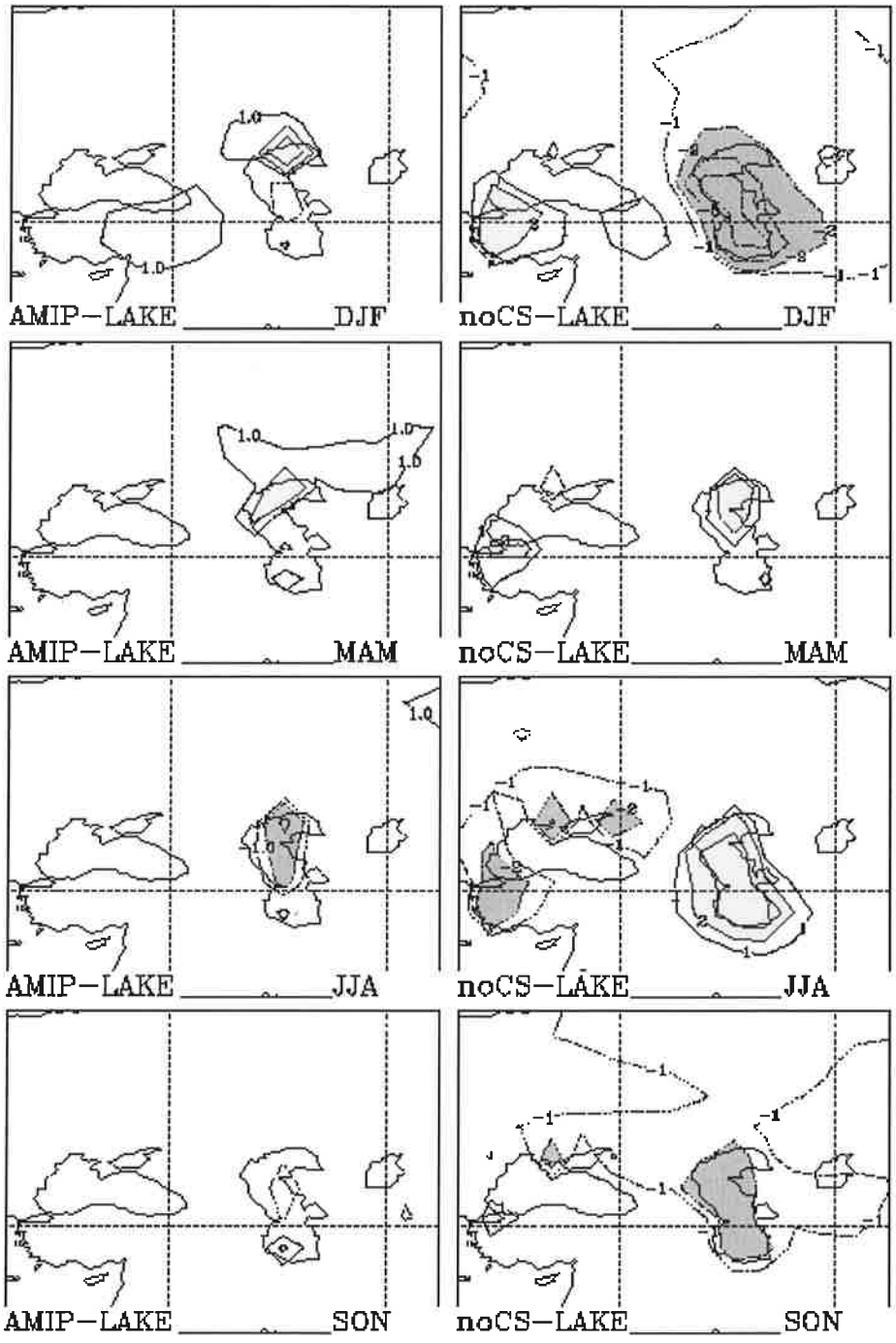

Figure 23 Surface temperature differences of the different runs for the four seasons. Solid (dotted) lines indicate plus (minus) 1, 2 and 5 degrees. Shaded area represents that the difference is larger than 2 degrees.

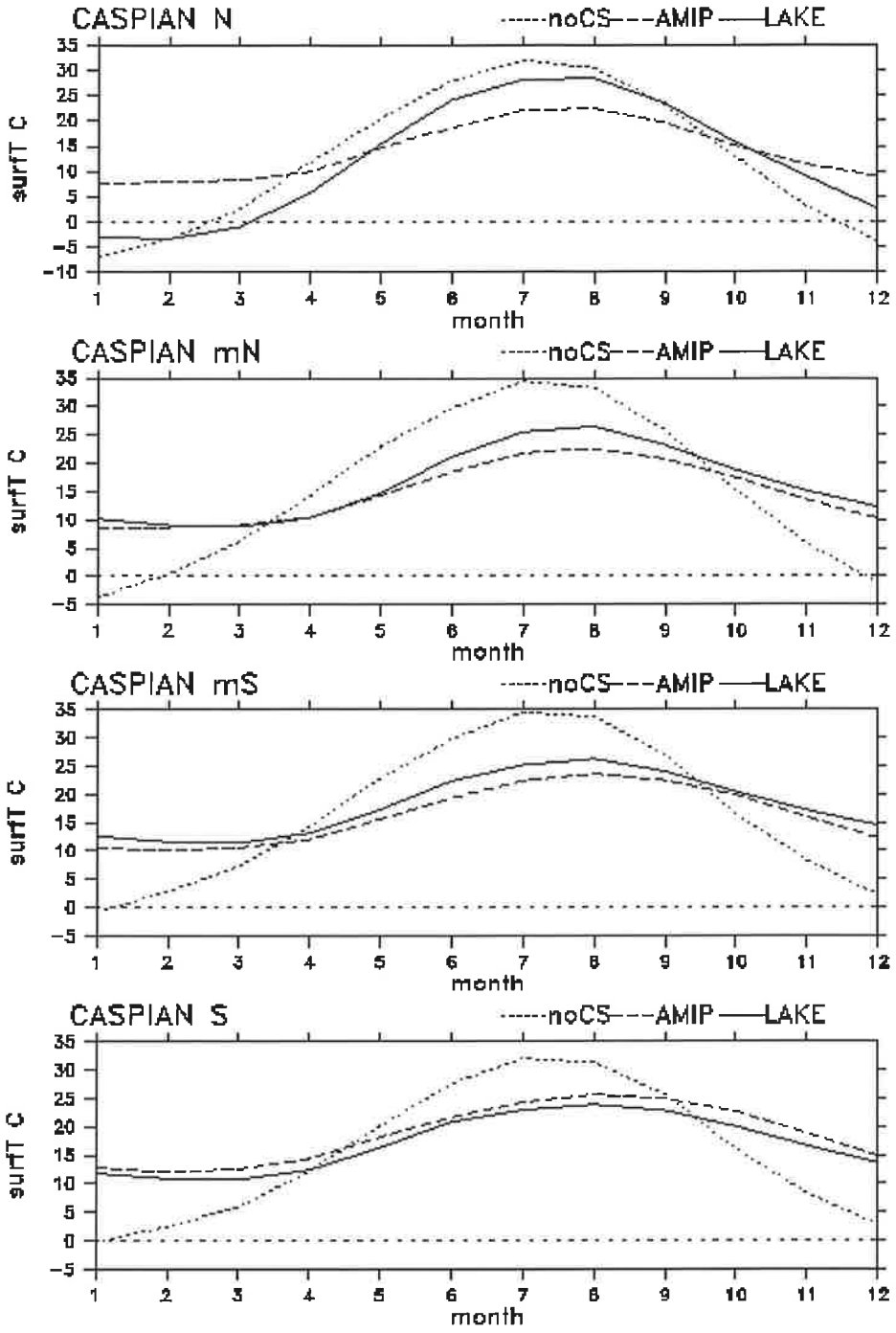

Figure 24 Annual cycles of SSTs simulated by different runs at the selected Caspian Sea grid points.

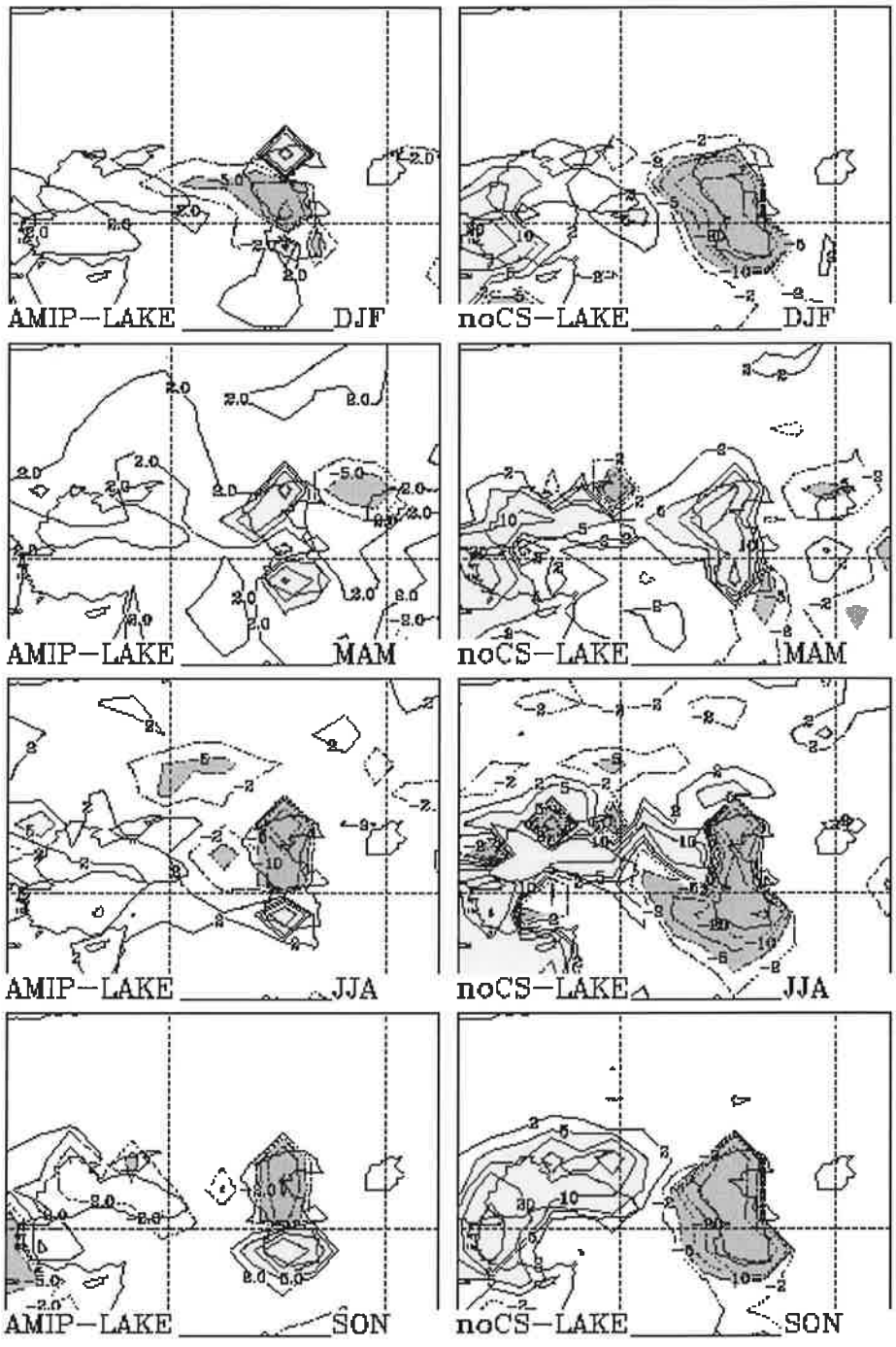

Figure 25 Latent heat flux differences of the different runs for the four seasons. Solid (dotted) lines indicate plus (minus) 1, 2, 5, 10 and 20 W/m^2. Shaded area represents that the difference is larger than 5 W/m^2.

This finding raises the question of statistical significance of the difference maps, which will be answered by Figure 26. Time series of latent heat flux are shown for the Black Sea and the Caspian Sea for spring and autumn, the two seasons with strongest signals in Figure 25. For the Caspian Sea there is not any question concerning the statistical significance as the curves representing the noCS and LAKE case are completely separated. During autumn (SON) the noCS case has hardly any soil moisture available to support some evaporation, the lower temperatures are probably of less importance. For the Black Sea one finds systematically higher values in the noCS case but less clear than for the Caspian Sea. During MAM there is only one year in which a LAKE value surpasses the mean noCS values and two years in which the noCS values surpass the mean LAKE value, for SON it is two or one year respectively. The LHFX depends not only on the SSTs but also on the surface wind and the humidity at the lowest atmospheric layer in a highly nonlinear way. This example shows that the Caspian Sea SSTs have an impact that is reaching beyond the Caspian Sea.

Surface temperature differences are further affecting the static stability of the atmosphere and by that it would influence the convective precipitation locally. In Figure 27 the maps of precipitation differences are shown and the correspondence - lower surface temperature leading to less precipitation - can generally be seen. However, during summer it is less strong and in autumn stronger because the massively lower local evaporation in the noCS case due to the absent of water. Also with the precipitation we see large-scale differences which are not caused locally. E.g. in winter there is less precipitation in the noCS case over western Turkey and southern Ukraine. Higher precipitation leads generally to lower surface temperatures and vice versa which can be seen for Turkey when comparing Figure 27 with Figure 23. However, the simulations of only 10 years are not sufficient to show that these differences are statistically significant.

Excessive or strongly reduced precipitation over the Caspian Sea must have an impact on the large-scale circulation. This is shown in Figure 28 for DJF, i.e. the season with the strongest signal, for the 700 hPa vertical velocity. The vertical velocity of the noCS case is very similar to the LAKE, and the AMIP cases. Sinking air can be found in the subtropical belt and rising air in the north of it. Figure 28 represents the difference maps between different case and it exhibits the impact of the Caspian Sea. Less precipitation in the noCS case is going hand in hand with reduced updraft over the Caspian Sea. A weak sinking motion compensates this over large areas of Asia. Both, the sinking and rising motions are statistically significant different in the LAKE and noCS runs for this season. For other seasons the signal is less clear and not significant.

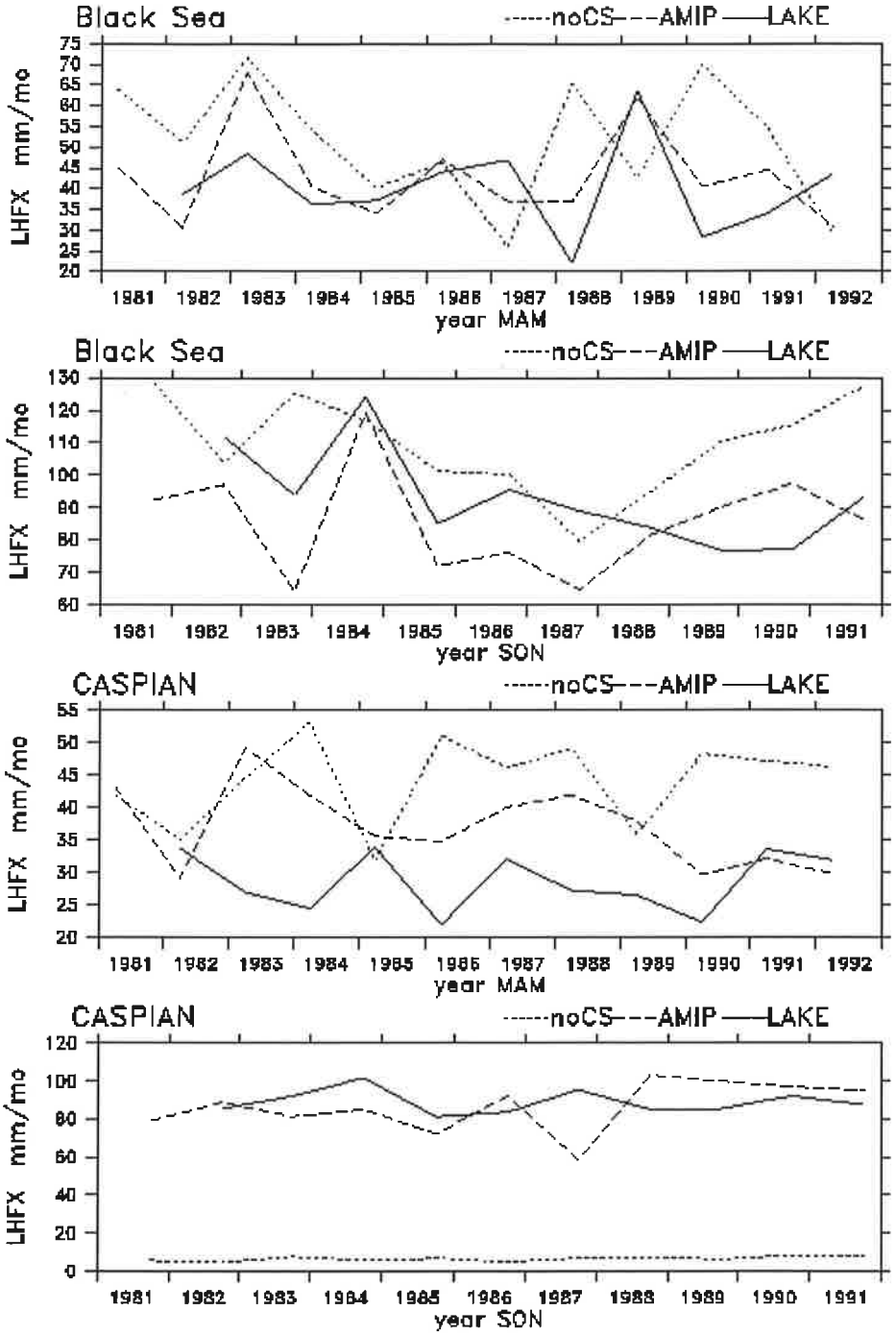

Figure 26 Annual cycles of latent heat flux simulated by different runs at the selected Caspian Sea grid points.

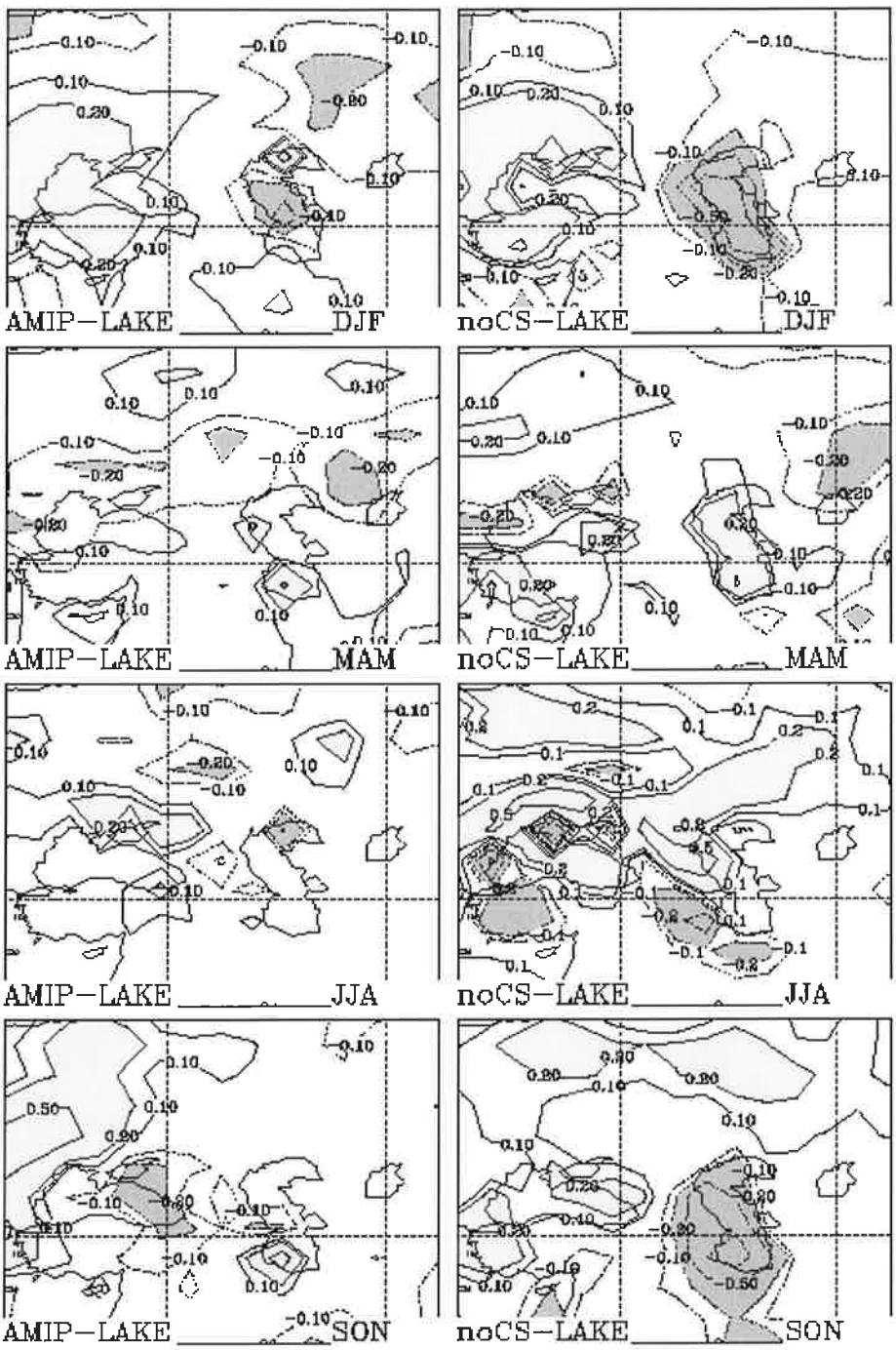

Figure 27 Precipitation differences of the different runs for the four seasons. Solid (dotted) lines indicate plus (minus) 0.1, 0.2, 0.5 and 1.0 mm/day. Shaded area represents that the difference is larger than 0.2 mm/day.

During winter also the differences of precipitation between the AMIP and LAKE run were shown to be largest and one can see also there a similar difference in the vertical velocity as in the LAKE - noCS case though with lower amplitudes (not shown).

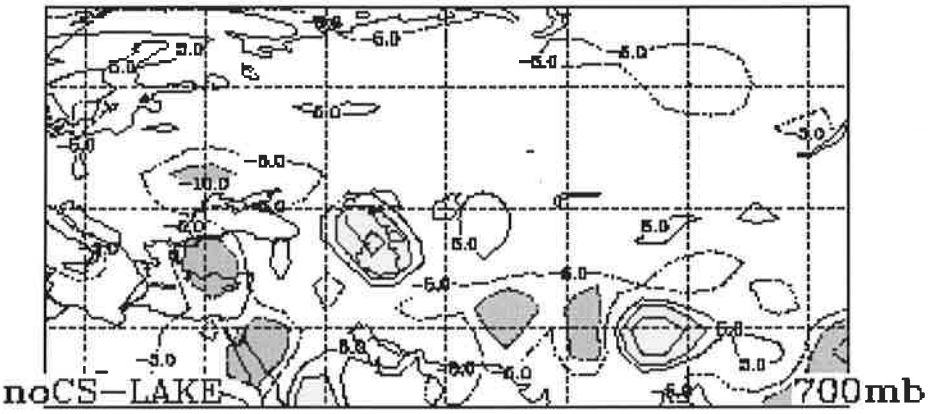

Figure 28 700 mb vertical velocity differences of the different runs for DJF. Solid (dotted) lines indicate plus (minus) 5 and 10 mPa/sec. Shaded area represents that the difference is larger than 10 mPa/sec.

4.3. ECHAM-5

Since the run of ECHAM-5+THMLAKE routine is still in progress, this section will be added in the future.

5. Conclusion

According to the simulation of ECHAM-4+THMLAKE model in the Caspian Sea, the result comparing to AMIP is satisfactory except in the most northern grid. Observations by SA and VMGO (1991) show the iced period during winter time in the northern Caspian Sea similar to the simulation which was not reproduced in the AMIP data set. During summertime, in the shallow waters of the most northern grid in the Caspian Sea the simulation gives almost 10℃ warmer values than AMIP. Comparison with observations at ports suggests that the reality lies somewhere between hot values, probably nearer to the simulation. Because of a lack of diffusion and advection terms, surplus energy stored in the most northern grid can not be transported to other grids and it becomes a hot spot in the Caspian Sea. The energy imbalance caused by lack of diffusion and advection term also exists in other grids. Some grids are hence slightly overestimated, while some are slightly underestimated. The defect of the lake subroutine can be improved by considering diffusion and advection terms.

Highly significant local impacts from the Caspian Sea on the atmosphere have been shown. For the extreme winter season also significant impacts on a larger scale could be demonstrated. The impacts in winter are very clear. Because the impact from temperature differences and from the availability of water for evaporation at the surface supported each other while in summer both effects canceled each other.

The impact on the evaporation is the most direct one. For this quantity the autumn shows the largest signal because in the no Caspian Sea case there is hardly any water left in the soil, leading to near zero evaporation while it is very large in both other simulations in which the Caspian Sea is represented. An example of non-linear effects on the evaporation has been shown as well, e.g. over the Black Sea in autumn, and such non-linear effects make it so difficult to show statistically significant impacts especially concerning the circulation.

Reference

Arakawa, A., 1972: Design of the UCLA General Circulation Model. *Tech. Rep.* **7**, Dept. of Meteorology, University of California, Los Angeles, 116 pp.

Arakawa, A. and Y. Mintz, 1974: The UCLA atmospheric general circulation model. Notes distributed at the workshop 25 March – 4 April 1974, Department of Meteorology, University of California, Los Angeles, California 90024.

Brutsaert, W., 1982: *Evaporation into the Atmosphere*. Reidel Pub. Co., 299 pp.

Carslaw, H.S. and J.C. Jaeger, 1959: *Conduction of Heat in Solids*. 2 nd., Oxford Press, 509 pp.

Chehbouni, A., E.G. Njoku, J.-P. Lhomme, and Y.H. Kerr, 1995: Approaches for averaging surface parameters and fluxes over heterogeneous terrain. *J. of Climate*, **8**, 1386-1393.

Deardorff, J.W., 1978: Efficient prediction of ground surface temperature and moisture, with inclusion of a layer of vegetation. *J. of Geophysical Research,* **83**, 1889-1903.

Dickinson, R.E., A. Henderson-Sellers, P.J. Kennedy, and W.F. Wilson, 1986: Biosphere-atmosphere transfer scheme (BATS) for the NCAR community climate model, *Tech. Note NCAR/TN275+STR*, Nat'l Center for Atm. Res., Boulder, Colorado.

Deutsches KilmaRechenZentrum (DKRZ), 1994: The ECHAM3 Atmospheric General Circulation Model. *Tech. Rep.* **6**, Deutsches KilmaRechenZentrum (German Climate Computer Center), Hamburg, Germany, 182 pp

Garratt, J.R., 1992: *The atmospheric boundary layer*. Cambridge Univ. Press, 316 pp.

Gates, L.W., 1992: AMIP: The Atmospheric Model Inter-comparison Project. *Bull. Am. Meteorology Soc.*, **73**, 1962-1970.

Hostetler, S.W., G.T. Bates, and F. Giorgi, 1993: Interactive coupling of a lake thermal model with a regional climate model. *J. of Geophysical Research*, **98**, 5045-5057.

Jin, M., R.E. Dickinson, and A.M. Vogelmann, 1997: A comparison of CCM2-BATS skin temperature and surface-air temperature with satellite and surface observations. *J. of Climate*, **10**, 1505-1524.

Kosarev, A. N., and E. A. Yablonskaya, 1994: The Caspian Sea. SPB

academic publ., The Hague, The Netherlands, 260 pp.

Lean, J., 1989: Contribution of ultraviolet irradiance variations to changes in the Sun's toatl irradiance. *Science*, **244**, 197-200.

Liang, X., D. P. Lettenmaier, E.F. Wood, and S.J. Burges, 1994: A simple hydrologically based model of land surface water and energy fluxes for general circulation models. *J. of Geophysical Research*, **99** (D7), 14415-14428.

List, R.J., 1971: *Smithsonian Meteorological Tables*, Smithsonian Institution Press, City of Washington, 6th Ed., 5th Reprint, 527 pp.

Oke, T.R., 1987: *Boundary Layer Climates*. 2 ed., Methuen Pub. Co., 435 pp.

Paltridge, G.W., and Platt, C.M.R., 1976: *Radiative Processes in Meteorology and Climatology*. Elsevier, New York.

Roeckner, E., K. Arpe, L. Bengtsson, M. Christoph, M. Claussen, L. Dumenil, M. Esch, M. Giorgetta, U. Schlese, and U. Schulzweida, 1996: The atmospheric general circulation model ECHAM-4: Model description and simulation of present-day climate. *Rep.* 218, Max-Planck-Institute for Meteorology, Hamburg, Germany, 90 pp.

Satterlund, D.R., 1979: An improved equation for estimating long-wave radiation from atmosphere. *Water Resources Research*, **15**, 1649-1650.

Sellers, P.J., Y. Mintz, Y.C. Sud, and A. Dalcher, 1986: A simple biosphere model (SiB) for use within general circulation models. *J. Atm. Sci.*, **43**, 505-531.

----------, J.L. Dorman, 1987: Testing the simple biosphere model (SiB) using point micrometeorological and biophysical data. *J. Clim. Appl. Meteor.* **26**, 622-651.

----------, D.A. Randall, G.J. Gollatz, J.A. Berry, C.B. Field, D.A. Dazlich, C. Zhang, G.D. Collelo, and L. Bounoua, 1996: A revised land surface parameterization (SiB2) for atmospheric GCMs. Part I: model formulation. *J. of Climate*, **9**, 676-705.

Shuttleworth, W.J., 1989: Micrometeorology of temperate and tropical forest, *Phil. Trans. Roy. Soc. London* **B324**, 299-334.

SA and VMGO (Headquarter of Soviet Army and Voeikov Main Geophysical Observatory), 1991: *Altas of hydrometeorological Data, Europe*. 1. Army Publ.: Mosco, (in Russia)

Stull, R.B., 1973: Inversion rise model based on penetrative convection. *J. of the Atmospheric Sciences*, **30**, 1092-1099.

Swinbank, W.C., 1963: Long-wave radiation from clear skies. *Quart. J. Royal Meteorol. Soc.*, **89**, 339-348.

Tsuang B.-J., and H.-C. Yuan, 1994: The ideal numerical surface thickness to determine ground surface temperature and schemes comparison. *Atmospheric Sciences*, **21**, 189-218, Chinese Meteorology Soc.

----------, and F.-J. Wang, 1993: Land surface parameterization for atmospheric models, *Atmospheric Sciences.* **21**, 137-157, Chinese Meteorology Soc.

----------, submitted: Determining function's mean of periodical data in the frequency domain.

Wallace, J.M., and P. V. Hobbs, 1977: *Atmospheric Science – An Introductory Survey.* Academic Press, 467 pp.